PLOS PATHOGENS

RESEARCH ARTICLE

Interactions between copper homeostasis and the fungal cell wall affect copper stress resistance

Corinna Probst[1,2,3], Sarela Garcia-Santamarina[2,3¤a], Jacob T. Brooks[4], Inge Van Der Kloet[1,2,3], Oliver Baars[5], Martina Ralle[6], Dennis J. Thiele[2,3,7¤b], J. Andrew Alspaugh[1,2]*

1 Duke University School of Medicine, Departments of Medicine, Durham, North Carolina, United States of America, **2** Genetics/Microbiology Department, Duke University School of Medicine, Durham, North Carolina, United States of America, **3** Pharmacology/Cancer Biology Department, Duke University School of Medicine, Durham, North Carolina, United States of America, **4** Department of Physics and Astronomy Department, University of North Carolina at Chapel Hill, Chapel Hill, North Carolina, United States of America, **5** Department of Entomology and Plant Pathology, North Carolina State University, Raleigh, North Carolina, United States of America, **6** Department of Molecular and Medical Genetics, Oregon Health and Science University,Portland, Oregon, United States of America, **7** Biochemistry Department; Duke University School of Medicine, Durham, North Carolina, United States of America

¤a Current address: Instituto de Tecnologia Quimica e Biologica, Universidade Nova de Lisboa, Oeiras, Portugal
¤b Current address: Sisu Pharma, Inc. Chapel Hill, North Carolina, United States of America
* andrew.alspaugh@duke.edu

Citation: Probst C, Garcia-Santamarina S, Brooks JT, Van Der Kloet I, Baars O, Ralle M, et al. (2022) Interactions between copper homeostasis and the fungal cell wall affect copper stress resistance. PLoS Pathog 18(6): e1010195. https://doi.org/10.1371/journal.ppat.1010195

Editor: Chad A. Rappleye, Ohio State University, UNITED STATES

Received: December 13, 2021

Accepted: May 31, 2022

Published: June 23, 2022

Data Availability Statement: All relevant data are within the manuscript and its Supporting Information files.

Funding: This work was supported by the National Science Foundation (award number ECCS-2025064), the National Science Foundation (award number ECCS-1542015), and the NIH core grant S10RR025512 (MR). This work was also supported by funding from the National Institute of Health: NIAID R01 AI074677 (JAA) and NIGMS R01GM041840 (DJT and JAA) and the German

Abstract

Copper homeostasis mechanisms are essential for microbial adaption to changing copper levels within the host during infection. In the opportunistic fungal pathogen *Cryptococcus neoformans* (*Cn*), the *Cn* Cbi1/Bim1 protein is a newly identified copper binding and release protein that is highly induced during copper limitation. Recent studies demonstrated that Cbi1 functions in copper uptake through the Ctr1 copper transporter during copper limitation. However, the mechanism of Cbi1 action is unknown. The fungal cell wall is a dynamic structure primarily composed of carbohydrate polymers, such as chitin and chitosan, polymers known to strongly bind copper ions. We demonstrated that Cbi1 depletion affects cell wall integrity and architecture, connecting copper homeostasis with adaptive changes within the fungal cell wall. The *cbi1*Δ mutant strain possesses an aberrant cell wall gene transcriptional signature as well as defects in chitin / chitosan deposition and exposure. Furthermore, using *Cn* strains defective in chitosan biosynthesis, we demonstrated that cell wall chitosan modulates the ability of the fungal cell to withstand copper stress. Given the previously described role for Cbi1 in copper uptake, we propose that this copper-binding protein could be involved in shuttling copper from the cell wall to the copper transporter Ctr1 for regulated microbial copper uptake.

Research Foundation Postdoctoral Fellowship grant PR 1727/1-1 (CP). The funders had no role in study design, data collection and analysis, decision to publish, or preparation of the manuscript.

Competing interests: The authors have declared that no competing interests exist.

Author summary

Microorganisms must be equipped to readily acquire essential micro-nutrients like copper from nutritionally poor environments while simultaneously shielding themselves from conditions of metal excess. We explored mechanisms of microbial copper homeostasis in the human opportunistic fungal pathogen *Cryptococcus neoformans* (*Cn*) by defining physiological roles of the newly described copper-binding and release protein *Cn* Cbi1/Bim1. Highly induced during copper limitation, Cbi1 has been shown to interact with the high-affinity copper transporter Ctr1. We defined Cbi1-regulated changes in the fungal cell wall, including controlling levels and surface exposure of the structural carbohydrates chitin and chitosan during copper and host-derived stress. These polysaccharides are embedded deeply in the cell wall and are known to avidly bind copper. Our data suggest a model in which the fungal cell wall, especially the chito-oligomer layer, serves as a copper-binding structure. Also, alterations in the cell wall polysaccharide content affect the ability to withstand excess copper. Given its ability to bind and release copper, the Cbi1 protein likely shuttles copper from the cell wall to copper transporters for regulated copper acquisition.

Introduction

Metal ions serve important and varied roles in the host-pathogen interaction. Transition metals, such as copper and iron, are essential micronutrients for both the host and pathogen, required as co-factors for cellular respiration and other central cell processes [1,2]. However, non-bound metal ions can be very cytotoxic. The requirement that microbial cells have ready access to non-toxic levels of transition metals governs a host process called "nutritional immunity". In this process, the host starves invading microbial pathogens by sequestering essential metals under certain conditions. Conversely, the host may actively bombard the pathogen with toxic levels of metals in other conditions. Nutritional immunity is best studied within microbe-containing macrophages in which Mn, Fe, and Zn are typically restricted by the host, while toxic levels of Cu are actively transported into the phagolysome by the ATP7A copper pump [3].

The genes that control copper homeostasis in fungi are under tight transcriptional control in response to extracellular copper concentrations. In contrast to many other fungi, the human fungal pathogen *Cryptococcus neoformans* (*Cn*) has a single transcription factor, Cuf1, that regulates the transcriptional response to both copper excess and copper starvation [4]. Within the Cuf1 regulon, one of the most highly induced genes during copper starvation is *Cn CBI1/BIM1* (CNAG_02775), encoding a GPI-anchored protein that interacts with the Ctr1 high-affinity Cu^{+} transporter [4,5]. The *Cn* Cbi1 copper binding and release protein, previously named Bim1, is required for growth in low copper conditions and therefore for effective brain colonization by this neuropathogenic yeast [5]. Cbi1 shares limited homology with lytic polysaccharide monooxygenase (LPMO) proteins that cleave glycosidic bonds within complex carbohydrates such as cellulose, starch, and chitin. Also similar to LPMOs and copper chaperones, *Cn* Cbi1/Bim1 binds copper in a histidine brace region, and it releases copper in reponse to low levels of hydrogen peroxide [6]. However, the purified *Cn* Cbi1/Bim1 protein does not possess the redox activity associated with most sugar-modifying enzymes [6,7]. It also lacks recognizable polysaccharide binding sites present in LPMOs [6,7]. Its specific function in Ctr1-mediated uptake of copper is therefore unclear. Based upon previous data, it has been proposed that *Cn* Cbi1/Bim1 acts as an intermediary copper binding protein, delivering

copper to Ctr1 for cellular copper acquisition. However, the details of this activity and the source of the copper bound by *Cn* Cbi1/Bim1 are not yet defined [5].

The *Cryptococcus* cell wall is a dynamic structure at the interface between the fungus and its external environment. The basal layer of fungal cell walls is composed primarily of chito-oligomers such as chitin and chitosan, which form a highly cross-linked and rigid structure near the plasma membrane. More superficial layers include other carbohydrates such as α- and β-glucans, as well as mannosylated proteins [8]. During infection and other periods of cell stress, *Cryptococcus* species remodel the cell wall to promote microbial survival under changing environmental conditions. During infection, these adaptive cell wall changes include facilitating the incorporation of the antioxidant pigment melanin, promoting the attachment of an anti-phagocytic capsule, and masking immunogenic cell wall epitopes to avoid immune recognition [9–12]. Several host-relevant signals are required for the induction of this type of fungal cell wall remodeling, including host temperature and the relatively alkaline pH encountered during infection [9,13]. However, it is not well understood how metal stress and nutritional immunity responses affect the fungal cell wall, or if the fungus actively remodels its cell surface in response to those stresses.

Components of fungal cell walls, especially chitin and chitosan, have been previously demonstrated to effectively chelate environmental divalent metal ions such as Cu^{2+} [14,15] but the physiological importance to the microbe of metal chelation by the fungal cell wall is poorly understood. To further explore the interaction between copper homeostasis and the fungal cell wall, we analyzed the cell wall remodelling response in the *cbi1*Δ mutant strain. We first characterized the role of Cbi1 in the transcriptional signatures of *Cn* cell wall-regulating genes. We also defined the physiological effects of mutations in proteins involved in copper homeostasis on the composition and integrity of the cell wall. Since the *Cn* cell wall is essential for the proper establishment of several factors associated with virulence, we determined how copper acquisition and homeostasis affect the expression of these specific microbial phenotypes. These studies suggest that copper availability affects the architecture and integrity of the fungal cell wall, processes likely required for microbial adaptation to host-like nutritional environments. Based upon our data we propose a dual role for the fungal cell wall in protecting *C. neformans* against the presence of toxic levels of copper and providing a source of metal ion availability during copper starvation.

Results

The transcription factor Cuf1 regulates cell wall integrity in response to cellular copper levels through the Cbi1-Ctr1 copper uptake complex

A recent study identified the *C. neoformans* Cuf1-dependent copper regulon in response to both copper deficiency and copper excess [4]. During copper deficiency, the most upregulated Cuf1-dependent transcripts represent genes involved in copper uptake, including those encoding for the high-affinity copper transporters Ctr1 and Ctr4 and the newly identified Cbi1 protein [4]. Previously referred to as *Cn* Bim1, this protein has been renamed Cbi1 (**C**u-**bi**nding and release protein 1) to reflect its known biochemical activities [6,7], and to recognize the previously described *Cn* Bim1 microtubule-binding protein involved in filamentous growth [16]. Besides genes involved in classical copper homeostasis pathways, this study identified many genes within the *Cn* Cuf1-copper regulon with functions associated with maintenance of the fungal cell surface and cell wall [4,5] (S1 Table). Among these copper regulated cell wall synthesis genes were two of the eight known chitin synthase genes (*CHS5*, *CHS7*), the chitin deacetylase 2 gene (*CDA2*), and three β-1,3-glucan modulating genes (CNAG_05458, CNAG_05138, CNAG_06636), directly connecting Cuf1-driven transcriptional regulation of

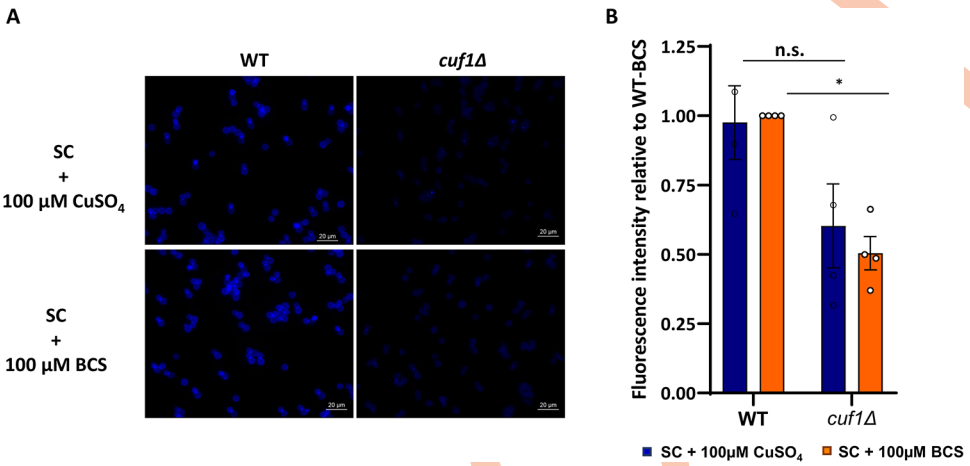

Fig 1. High and low Cu stressed *cuf1Δ* cells show a decrease in cell wall chitin. **(A)** Calcofluor white (CFW) staining of WT and *cuf1Δ* cells in high and low copper stress. Cells were cultivated at high copper stress (SC+ 100 μM $CuSO_4$) or low copper stress (SC + 100 μM BCS) for 12h at 30˚C and stained with CFW as a marker of total cell wall chitin/chitosan. **(B)** Quantification of CFW staining signal. Shown is the mean +/- SEM of the relative CFW intensity from 4 independent experiments. The CFW intensities were measured with ImageJ/Fiji and normalized to cell count. Shown is the relative CFW intensity (low copper WT set to 1). A 2-way ANOVA was performed from log transformed data using GraphPad Prism.

https://doi.org/10.1371/journal.ppat.1010195.g001

copper homeostasis to cell wall remodelling and synthesis. Therefore, to test the effects of *Cn* Cuf1 function on the fungal cell wall, we cultured the WT strain and the *cuf1Δ* mutant in presence of high Cu or low Cu stress (induced by the addition of the Cu^+-chelator bathocuproine-disulfonic acid (BCS)). We then analyzed the strains microscopically after staining with calcofluor white (CFW), a dye binding to the inner cell wall layer formed by chitin and chitosan [17] (Fig 1A and 1B). In both copper stress conditions we observed a decrease in CFW staining intensity in *cuf1Δ* mutant cells, suggesting lower chitin cell wall content.

The fungal cell wall is a dynamic structure required for viability, stress resistance, morphogenesis and virulence. Its composition is actively remodeled in response to various stress signals, and this process is controlled by conserved signaling cascades, including the cell wall integrity (CWI) pathway [18]. The cell wall stress experienced by the copper homeostasis mutants, specifically during copper deprivation, is reflected in transcriptional alterations in the CWI pathway. The *ROM2* gene encodes a guanine nucleotide exchange factor required for CWI pathway activation under conditions of cell stress [19]. Transcriptional induction of *ROM2* is therefore typically observed during conditions of cell wall stress. Comparative transcriptional analysis of the WT and *cuf1*Δ mutant revealed similar *ROM2* transcript levels between these two strains during copper sufficiency (Fig 2A). In contrast, *ROM2* transcript levels were 3-fold higher in the *cuf1*Δ strain compared to wildtype during copper starvation. A similar trend was observed for other components of the cell wall stress pathway such as *CRZ1* and *ROM20* (S1A and S1B Fig). Complementation of the *cuf1*Δ mutant with the *CUF1-FLAG* gene (*cuf1*Δ^C strain) restored the transcript levels to wildtype levels (Figs 2A and S1A and S1B). Taken together depletion of *Cn* Cuf1 directly effects the fungal cell wall in modulating the inner chitin layer (quantified through CFW staining) and causes increased cell wall stress specifically during copper deficiency.

To further analyze the impact of *CUF1* and other Cuf1-regulated copper homeostasis genes for maintaining cell wall integrity during copper deficiency, we assessed the sensitivity of the *cuf1*Δ, *cbi1*Δ, *ctr1*Δ and *ctr4*Δ strains to cell wall stressors in copper-replete and copper-deficient conditions. These stresses included calcofluor white (CFW, blocks chitin assembly),

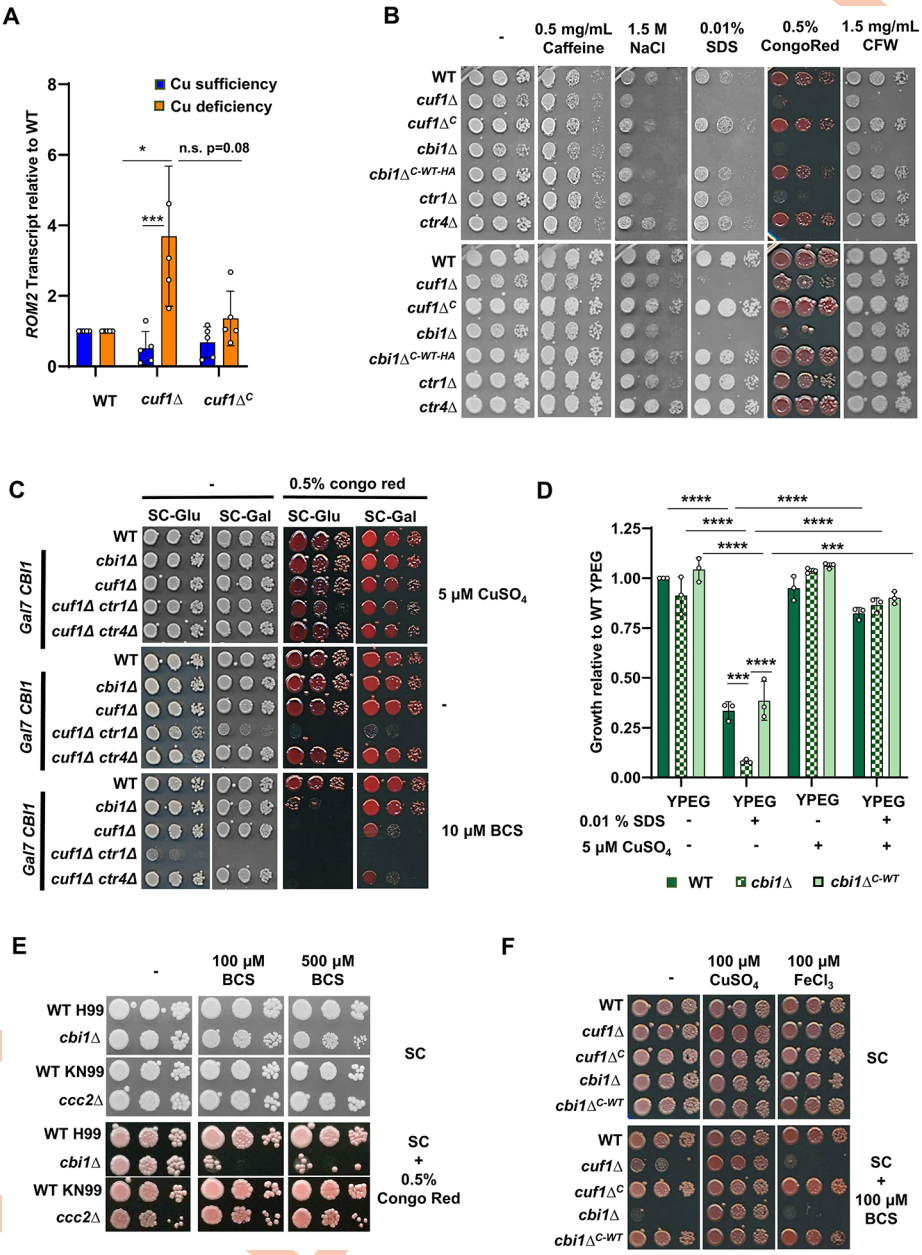

Fig 2. The Cuf1 transcription factor as well as it targets Cbi1 and Ctr1 are involved in maintaining cell wall integrity during copper deficiency. (A) Transcript abundance of the cell wall stress gene *ROM2* during copper deprivation. The WT, *cuf1*Δ and Cuf1-Flag complemented *cuf1*Δ^{C} strains were incubated in either high copper (SC medium with 1 mM $CuSO_4$ for 1h at 30˚C) or low copper (SC medium with 1 mM BCS for 6h at 30˚C) conditions. Quantitative RT-PCR was used to assess relative *ROM2* transcript levels for each strain compared to the WT in each condition. Presented is the mean +/- SEM of the relative transcript levels of 5 biological replicates. A 2-way ANOVA was performed from log transformed data using GraphPad Prism. **(B)** Growth analysis in presence of cell wall/ surface stressors. Five-fold serial dilutions of cell suspensions for each strain were incubated on SC medium with 100 μM BCS, supplemented with indicated amounts of cell wall and cell surface stressors. Plates were incubated at 30˚C for 2-4d, and the figure shows a representative image from 3 independent experiments. **(C)** *GAL7* promoter-driven expression of Cbi1 in different mutant strain backgrounds during cell wall stress. Five-fold serial dilutions of cell suspensions for each strain were incubated on SC medium with indicated copper concentrations, in the presence or absence of the cell wall stressor Congo red, on SC medium with either glucose (SC-Glu) (*CBI1*-repressing conditions) or galactose (SC-Gal) (*CBI1*-inducing conditions) as carbohydrate source. Plates were incubated at 30˚C for 3d. This figure shows a representative image from 3 independent spotting experiments. **(D)** The WT, *cbi1*Δ, and *cbi1*Δ (*cbi1*Δ$^{C\text{-}WT}$) complemented strains were incubated in YP medium with the non-fermentable carbon sources ethanol and glycerol (YPEG) in presence and absence of the cell wall stressor SDS, and with or without the addition of 5 μM $CuSO_4$.

Growth was assessed by OD_{600} of the cultures after 72h of incubation at 30˚C and normalized to WT growth in YPEG media. Presented is the mean +/- SEM of the relative growth rates of 3 biological replicates. 1-way ANOVA was performed from log transformed data using GraphPad Prism. **(E)** Impact of the *ccc2*Δ mutation on growth in presence of the cell wall stressor Congo red. Five-fold serial dilutions of cell suspensions for each strain were incubated on SC medium with and without the addition of Congo red, and with 100 μM or 500 μM BCS as copper chelation. Plates were incubated at 30˚C for 2-4d. **(F)** Copper restoration of cell wall stressor sensitivity of *cbi1*Δ cells. Five-fold serial dilutions of cell suspensions for each strain were incubated on SC medium with and without 100 μM BCS, and with the addition of either 100 μM $CuSO_4$ or 100 μM $FeCl_3$. Plates were incubated at 30˚C for 3d. This figure shows a representative image from 3 independent spotting experiments.

https://doi.org/10.1371/journal.ppat.1010195.g002

Congo red (impairs assembly of cell wall polymers, mainly chitin), caffeine (impacts PKA-mediated signal transduction), SDS (cell surface/ membrane stressor) and NaCl (osmotic stressor) [20–22]. We did not observe any growth phenotypes for the mutant strains in the presence of these cell wall stressors under copper-replete conditions (S1C Fig). In contrast, during copper starvation induced by the extracellular copper (I) chelator bathocuproinedisulfonic acid (BCS) (100μM), the *cuf1*Δ *and cbi1*Δ strains exhibited strong growth inhibition compared to WT on NaCl, SDS, Congo red and CFW-containing media (Fig 2B). Even at more modest levels of copper chelation (10 μM BCS), the *cuf1*Δ *and cbi1*Δ strains exhibited growth inhibition on Congo red-containing media (Fig 2C). Additionally, the Ctr1 copper transporter was similarly required for survival during copper deprivation in the presence of NaCl and CFW, but not in the presence of SDS. No cell wall stress-associated growth defect was noted for the *ctr4*Δ copper transporter mutant strain (Fig 2B), supporting prior observations that the Ctr1 and Ctr4 high affinity copper transporters serve overlapping but non-redundant functions in *Cn* copper homeostasis [23]. Growth inhibition of the *cuf1*Δ and *cbi1*Δ strains was complemented by expressing epitope-tagged versions of these proteins in the respective mutant strains [Cuf1-Flag in *cuf1*Δ (cuf1Δ^{C}) or Cbi1-HA in *cbi1*Δ (*cbi1*$\Delta^{C\text{-}WT\text{-}HA}$)]. These results suggest an interaction between copper abundance/homeostasis and *Cn* cell wall stress resistance.

To further explore the relationships among the *Cn* copper homeostasis proteins in cell wall integrity, especially the less well-characterized Cbi1 protein, we conditionally overexpressed the *CBI1* gene in a series of individual and double mutant strains (Fig 2C). Galactose-mediated overexpression of the p*GAL7-CBI1* allele fully complemented the copper-dependent cell wall growth defect of the *cbi1*Δ mutant, and partially that of the *cuf1*Δ strain. In contrast, overexpression of *CBI1* was unable to restore cell wall integrity to strains with a *ctr1*Δ mutation. These results are consistent with prior studies suggesting that Cbi1 and Ctr1 are components of a common copper transporter complex [5]. Additionally, these findings indicate that Cuf1 controls many Cu-regulated cell wall processes, but that defective Cbi1 function is likely responsible for much of the loss of cell wall integrity in the *cuf1*Δ mutant.

We also assessed *Cn* copper-dependent cell wall integrity phenotypes using an alternative method of copper limitation to extracellular copper chelation by BCS. We incubated the *Cn* strains in media containing ethanol and glycerol as sole carbon sources. Growth on these non-fermentable carbohydrates is only supported by cellular respiration, effectively shunting intracellular copper into the mitochondria to the copper-dependent enzymes required for oxidative phosphorylation. Incubation of the WT and *cbi1*$\Delta^{C\text{-}WT}$ strains in YPEG + 0.01% SDS caused a ~40% growth reduction, and an even more severe reduction of growth (~90%) in the *cbi1*Δ strain (Fig 2D). This growth impairment was complemented in all strains by supplementation with $CuSO_4$, suggesting that shuttling of copper from other pathways towards respiration influences the ability of *Cn* to withstand cell surface stress. Depletion of Cbi1 further decreased cell fitness under these conditions.

We also tested the cell wall integrity of the *Cn ccc2*Δ mutant, a strain defective in copper transport withinin the secretory pathway and subsequent altered metalation of secreted proteins [2,24]. A modest growth defect on Congo red was observed for the *ccc2*Δ strain, and the defect developed independent of copper availability (Fig 2E). These results suggest that defective copper loading of enzymes in the secretory compartment is likely not the cause of the most prominent *Cn* cell wall phenotypes observed during copper deficiency.

The Cfo1 ferroxidase is a copper-dependent enzyme involved in high-affinity iron acquisition [25]. Therefore, loss-of-function mutations in Cuf1 or other components of the *Cn* copper uptake machinery would be predicted to affect intracellular iron concentrations as well as copper levels. Additionally, previous studies demonstrated that iron homeostasis is important for proper fungal cell wall and membrane architecture [26,27]. We therefore analyzed the effects of exogenous copper or iron on the BCS-induced cell wall phenotypes of the *cbi1*Δ and *cuf1*Δ mutants. Individual supplementation of the growth medium with copper, but not iron, restored growth to the *cbi1Δ* and *cuf1Δ* strains in the presence of cell wall stress and copper depletion (Fig 2F). This finding suggest that the observed cell wall stress phenotype is not solely the effect of iron starvation caused by a decrease in copper availability but directly linked to copper limitation.

Changes in *Cn* cell wall composition in response to defective copper homeostasis

To further characterize the specific role of Cbi1 in cell wall homeostasis during copper stress, we used transmission electron microscopy (TEM) to characterize the cell wall architecture of the wildtype (WT) and *cbi1*Δ strains incubated in both copper-sufficient and copper-deficient growth conditions (Fig 3A–3C). In copper-sufficient conditions the *Cn* WT cell wall consists of two layers characterized by differing electron density [28–30]. Extracellular copper sequestration by the highly copper-specific chelator BCS resulted in decreased electron density in the innermost cell wall layer composed primarily of chitin and chitosan (Fig 3A and 3C). These chito-oligomers efficiently bind divalent metals (including copper ions), consistent with the higher electron density of this cell wall layer during copper sufficiency [14,15]. The cell wall of the *cbi1*Δ mutant strain was similar to WT during copper sufficiency, displaying distinct layers based on electron density. However, the copper-starved *cbi1*Δ strain demonstrated a reduction in total cell wall thickness compared to both the WT strain and the copper-sufficient *cbi1*Δ cells (Fig 3B). Also in contrast to WT, there was no reduction in the inner cell wall electron density in the *cbi1*Δ mutant strains during copper deficiency (Fig 3A and 3C).

The ultrastructural changes observed in the *cbi1*Δ strain cell wall during copper starvation were not due to altered cell viability. Although the *cbi1*Δ strain demonstrated a defect in proliferation during copper deficiency, we observed no decrease in *cbi1*Δ cell viability during the first 24 hours, as assessed by quantitative culture (S1D and S1E Fig). We also assessed the effective "copper state" of the WT and *cbi1*Δ strains in the conditions chosen for copper sufficiency (10 μM $CuSO_4$) and deficiency (250 μM BCS) by quantifying transcript levels of the *CMT1* metallothionein gene (induced during high copper states) and the *CTR4* copper transporter gene (induced during copper starvation) (S1F Fig). Both the WT and *cbi1Δ* strains demonstrated a strong induction of *CTR4* expression, but not of the *CMT1* transcript, indicating effective induction of copper deficiency by BCS treatment compared to the copper sufficient growth conditions.

We performed ICP-MS-based metal quantification of cell-associated copper and iron both WT and *cbi1Δ* strains in copper sufficient and deficient conditions (Fig 3D and 3E). As predicted by the role of Cu-depending proteins in cellular iron import, both WT and *cbi1Δ* cells

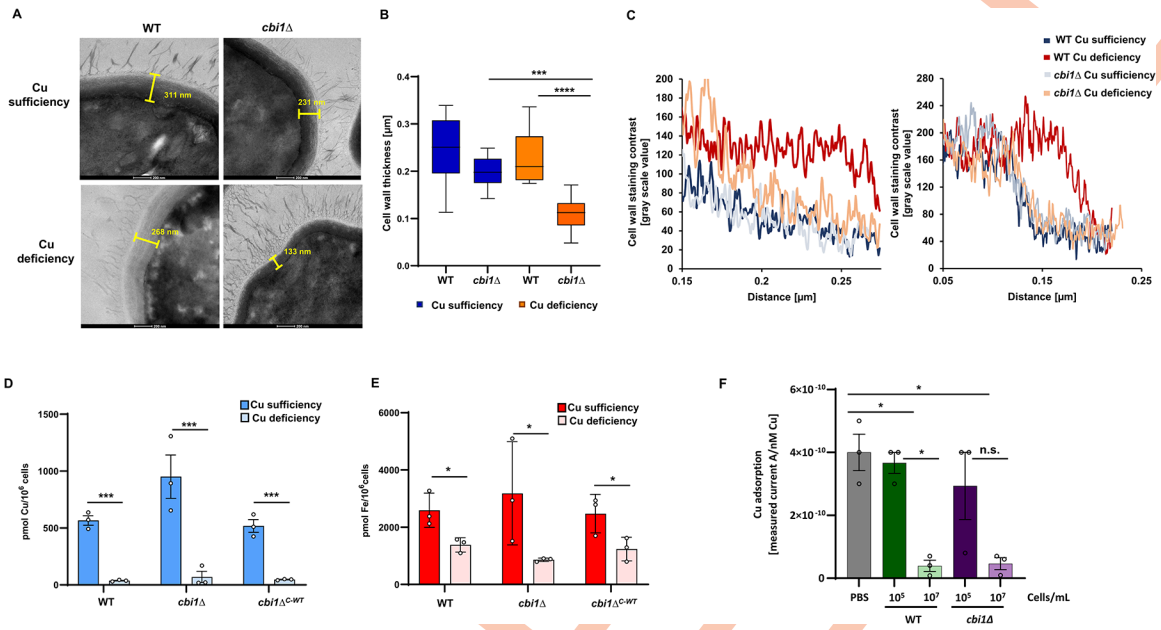

Fig 3. Copper deficient *cbi1Δ* cells show a to WT distinct cell wall electron density pattern, which is not due to overall difference in cell associated copper levels or copper adsorption ability. Transmission electron microscopy (TEM) images of copper sufficient or deficient WT and *cbi1Δ* cells. The WT and *cbi1Δ* strains were incubated in YPD medium supplemented with 10 μM $CuSO_4$ (Cu sufficiency) or with 250 μM BCS (Cu deficiency) for 24h at 30˚C. **(A)** Representative images with representative cell wall thickness indicated (29000 x magnification). **(B)** Quantification of cell wall thickness. Measurements were performed using the ImageJ/Fiji measurement tool: Cu sufficiency-WT 10 cells, Cu sufficiency- *cbi1Δ* 8 cells, Cu deficiency-WT 11 cells and Cu deficiency-*cbi1Δ* 14 cells. A 1-way ANOVA was performed using GraphPad Prism from log transformed data. **(C)** Quantification of the cell wall staining intensity. Presented is the analysis of two sets of TEM images. The gray value was measured with ImageJ/Fiji and plotted against the distance along the cell wall from the inner cell surface. **(D-E)** ICP-MS based metal quantification of cell associated copper (D) and Iron (E) in pg metal per 10^6 cells. Indicated strains were grown in identical growth conditions to the TEM experiment. Presented is the average +/- SEM from 3 biological replicates. A 2-way ANOVA was performed from log transformed data using GraphPad Prism. **(F)** ASV analysis of copper adsorption by *Cn* cells. Indicated strains were grown under Cu starvation (YPD + 250 μM BCS) for 24h at 30˚C. Copper was titrated in 250 nM steps into 20 mL cell suspension of indicated concentration or PBS (= control). The peak height of the resulting current in each titration step was measured using the NOVA software (Autolab) and plotted against copper concentration. Linear regression was performed to determine slope of each titration experiment. Shown is the mean +/- SEM of the slopes determined by 3 independednt titration experiments. A ONE-Way ANOVA was performed from log transformed data.

https://doi.org/10.1371/journal.ppat.1010195.g003

show a similar pattern of reduced cell-associated copper and iron after BCS incubation. Therefore, the different pattern in electron density observed in copper starved WT and *cbi1Δ* cells cannot simply be explained by changes in total cell copper or iron levels. However, this type of ICP-MS analysis of total cellular metals is not sufficiently sensitive to discriminate between cell surface associated and intracellular metal accumulation in these small fungal cells.

To better investigate surface adsorption of copper by different *Cn* strains, we used anodic stripping voltammetry (ASV) with a Hanging Mercury Drop Electrode. ASV measures copper speciation based on reducibility at an electrode surface [31]. We expected Cu^{2+} adsorbed to the cell surface to be electrochemically inert due to Cu^{2+} chelation by cell wall polysaccharides which makes it kinetically inert for reduction and slow to diffuse to the electrode surface. Using two concentrations (10^5 or 10^7 cells/mL) of fungal cells in suspension in PBS, we observed a measurable adsorption of Cu^{2+} onto the *Cn* cell surface at the higher cell concentration compared to cell-free PBS. These finding shows that *Cn* cells readily adsorb Cu^{2+} ions on there cell surface with no major differences in adsorption capacity between the WT and *cbi1Δ* cell surface.

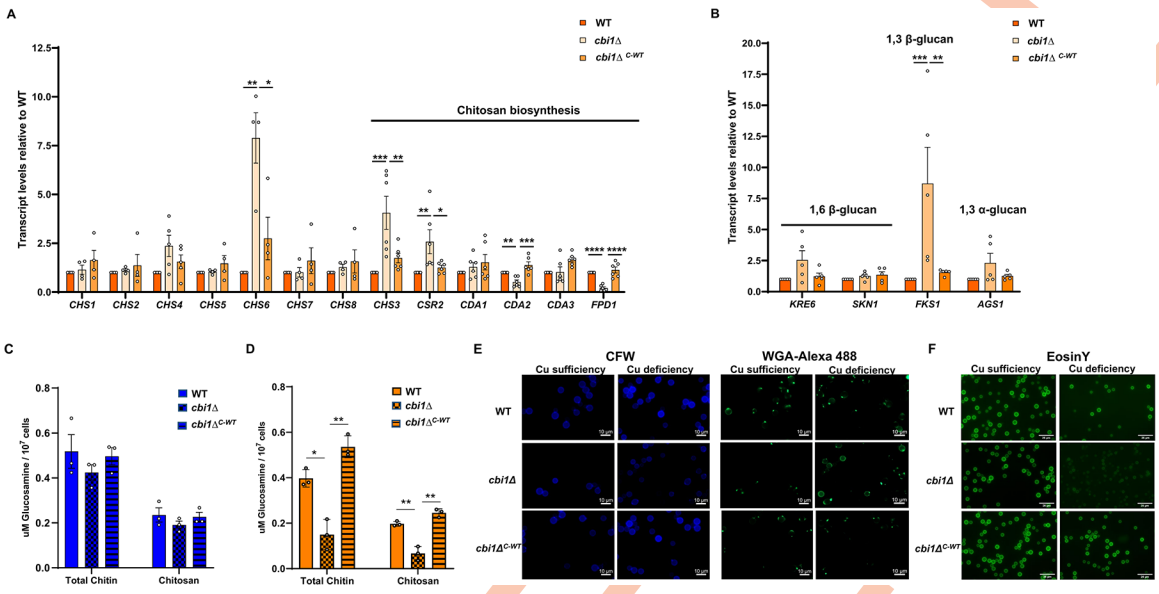

Fig 4. Cbi1-dependent cell wall gene transcript abundance and cell wall chitosan levels. (A)-(B) The WT, *cbi1*Δ mutant, and *cbi1*Δ$^{C\text{-}WT}$ complemented strains were incubated in YPD supplemented with 250μM BCS for 24h at 30˚C. Relative transcript abundance for cell wall genes involved in **(A)** chitin/chitosan synthesis or **(B)** glucan synthesis was assessed by quantitative RT-PCR and normalized to WT. Presented data is the mean +/- SEM of the relative transcript levels of 4 biological replicates. A 1-way ANOVA was performed from log transformed data using GraphPad Prism. **(C)-(D)** Chitin/chitosan quantification of copper sufficient (C) or deficient (D). The WT, *cbi1*Δ mutant, and *cbi1*Δ$^{C\text{-}WT}$ complemenbted strains were incubated for 24h in YPD+ 10 uM CuSO4 (copper sufficiency) or YPD +250 uM BCS (copper deficiency). MBTH-based chitin/chitosan quantification (μM glucosamin/10^7 cells) was performed for purified cell wall material. Data represent the mean +/- SEM of 3 biological replicates. A 1-way ANOVA was performed from log transformed data using GraphPad Prism. **(E)** The same strains incubated in identical conditions above were also assessed for chitin and chitosan by staining with calcofluor white (CFW) (total chitin/chitosan), wheat germ agglutin (WGA)-Alexa 488 (exposed chitin/chitosan), and **(F)** Eosin Y (chitosan). Representative images from at least three independent experiments are demonstrated.

https://doi.org/10.1371/journal.ppat.1010195.g004

Transcriptional changes in cell wall genes in response to copper status

Prior investigations have established a set of *C. neoformans* genes encoding enzymes involved in the synthesis and chemical modification of the major cell wall structural carbohydrates. These include 8 chitin synthetase genes (*CHS1-8*), 4 chitin deacetylase genes (chitin-to-chitosan conversion) (*CDA1-3*, *FPD1*), and the chitin synthase regulator-2 (*CSR2*). Genes involved in glucan synthesis include *KRE6* and *SKN1* (β-1,6-glucan), *FKS1* (β-1,3-glucan) and *AGS1* (α-1,3-glucan) [8]. To investigate how copper availability and Cbi1 might affect cell wall carbohydrate homeostasis, we measured transcript levels of these major cell wall synthesis genes in copper deficient wildtype (WT), *cbi1*Δ mutant, and *cbi1Δ*$^{C\text{-}WT}$ complemented strain (Fig 4A and 4B). Among the genes involved in chitin and chitosan synthesis, we observed significant increases in transcript abundance in the *cbi1*Δ mutant for *CHS6* (~7 fold), *CHS3* (~4 fold) and *CSR2* (~3 fold), while the chitin/chitosan deacetylase genes *CDA2* and *FPD1* were downregulated (Fig 2D). In addition to genes involved in chitin/chitosan biosynthesis, the transcript level of the β-1,3-glucan synthase *FKS1* gene was induced 8-fold. Changes in the expression of *KRE6* (β-1,6-glucan synthesis) and *AGS1* (α-1,3-glucan synthesis) were not statistically significantly altered (Fig 4B). These findings indicate that the copper-deficient *cbi1*Δ strain displays transcriptional changes in several cell wall polysaccharide synthesis genes, especially those associated with chitosan and β-1,3-glucan synthesis.

To explore the functional relevance of changes in *Cn* cell wall gene transcript abundance as a function of copper availability, we quantified β-glucan and chitin/chitosan levels in the WT, *cbi1Δ* mutant, and *cbi1Δ*$^{C\text{-}WT}$ complemented strains after incubation for 24h in copper-

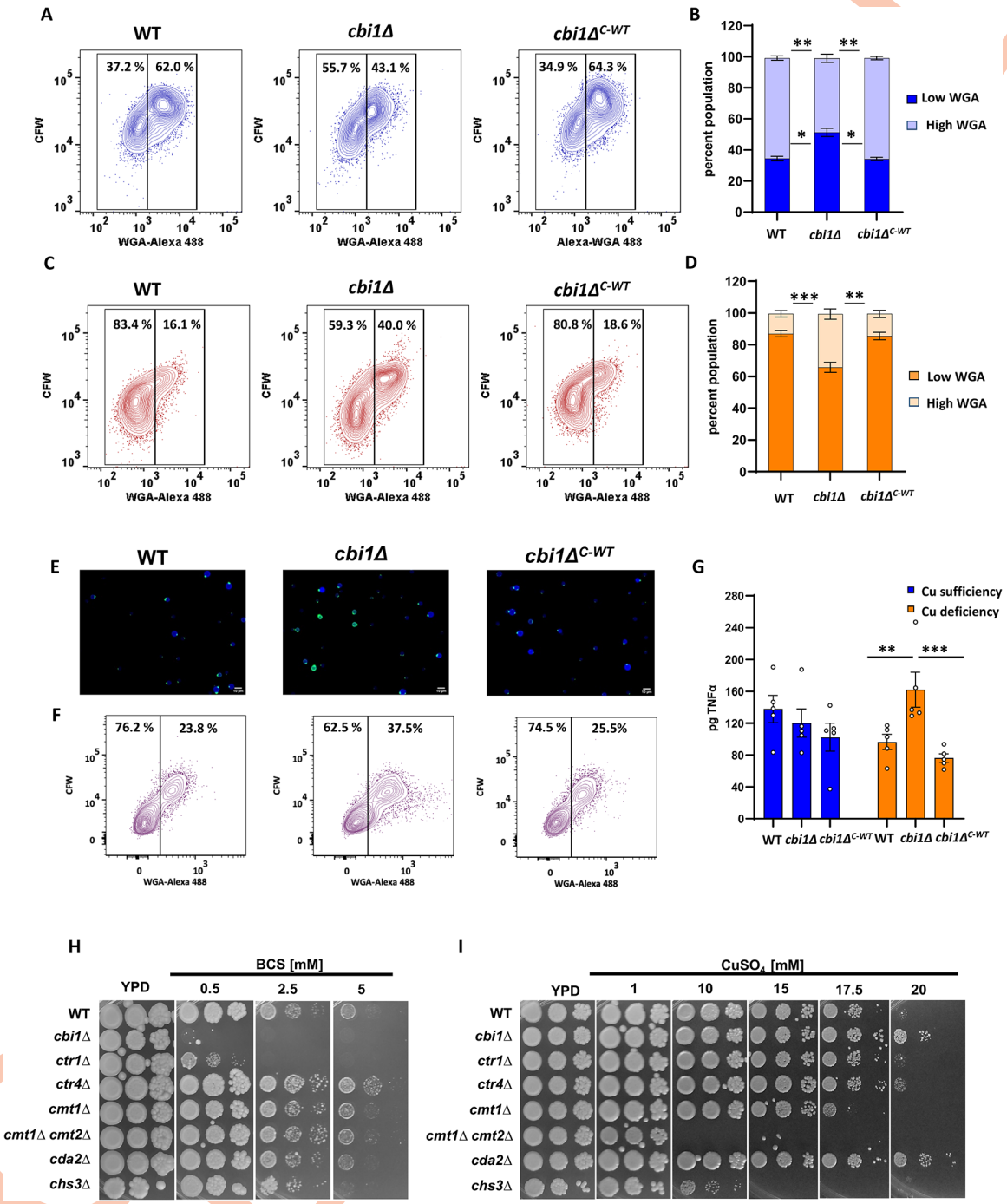

Fig 5. Cbi1 depletion effects chitin architecture during copper deficiency and host stress. (A)-(D) The WT, *cbi1*Δ mutant, and *cbi1*Δ$^{C\text{-}WT}$ complemented strains were incubated for 24h in YPD+ 10 uM CuSO4 (copper sufficiency) or YPD +250 μM BCS (copper deficiency), harvested, and double stained with CFW and WGA-Alexa 488. Stained cells were analyzed using a FACS Canto A Analyzer, and data were analyzed using Flow Jo. Representative data indicating percentage of total cells staining as "High WGA" (increased exposed chitin/chitosan) after incubation in copper-sufficiency **(A)** or copper-deficiency **(C)**. Quantification of three independent experiments for copper-sufficiency **(B)** or copper-deficiency **(D)** conditions. A 2-way ANOVA was performed from log transformed data using GraphPad Prism. **(E)-(F)** Cell wall analysis was performed for the WT, *cbi1*Δ mutant, and *cbi1*Δ$^{C\text{-}WT}$ complemented strains after incubation for 24h in CO_2-independent medium at 37˚C. Cells were analyzed microscopically using WGA-Alexa 488 staining **(E),** or by FACS analysis for High WGA cells per above **(F)**. **(G)** Macrophage activation assay upon infection with copper sufficient or deficient WT, *cbi1*Δ and *cbi1*Δ$^{C\text{-}WT}$ complemented cells. BMMs were harvested from A/J mice and co-incubated with *Cn* cells at an MOI of 10:1 (Cn:BMMs), followed by an ELISA-based quantification of TNF-α (pg) in the supernatant. Presented is the mean +/- SEM of 5

independent experiments. A 2-way ANOVA was performed from log transformed data using GraphPad Prism. **(I-J)** Five-fold serial dilutiuons of indicated strains were incubated on YPD medium supplemented with indicated amounts of BCS (copper starvation) **(I)** or $CuSO_4$ (toxic copper stress) **(J)**. Plates were incubated at 30˚C for 2-6d.

https://doi.org/10.1371/journal.ppat.1010195.g005

sufficient (YPD + 10 μM $CuSO_4$) and copper-deficient (YPD + 250 μM BCS) conditions. No significant changes were detected in total cell wall β-glucan between the WT and *cbi1*Δ cells in either growth condition (S2A Fig). However, the *cbi1*Δ mutant exposed to copper-deficiency displayed a greater than 50% reduction in total cell wall chito-oligomers due to a drastic reduction of chitosan compared to WT and complemented strains (Fig 4C and 4D). Therefore, the reduction of cell wall thickness and altered cell wall integrity in the *cbi1*Δ strain during copper starvation is, in part, likely due to a reduction in the inner cell wall chito-oligomer layer, especially chitosan.

In addition to measuring alteration in cell wall polysaccharide content, we also examined changes in the patterns of chitin and chitosan deposition using chitin- and chitosan-specific fluorescent stains. We double-stained Cu-sufficient and Cu-deficient *Cn* cells with Calcofluor white (CFW), a small molecule staining 1,3-β-and 1,4-β-polysaccharides of chitin/chitosan [17], and AlexaFluor488-conjugated wheat germ agglutin (WGA-Alexa 488), a lectin that binds exposed chito-oligomers [32,33]. Consistent with the reduction in total cell chitin/chitosan measured in the biochemical assays, we observed a similar reduction in CFW staining intensity of Cu-deficient *cbi1Δ* cells (Figs 4E and S2B). WGA staining of WT and *cbi1*$\Delta^{C\text{-}WT}$ complemented cells revealed exposed chito-oligomers primarily at regions of cell separation, budding sites, and bud scars. In contrast, the copper-deficient *cbi1Δ* cells demonstrated an enrichment of WGA-Alexa 488 staining globally around the cell surface. Our biochemical analysis of the *cbi1Δ* cell wall composition showed that the reduction in total chitin was primarily due to significant loss of chitosan. Therefore, to specifically stain for chitosan we used EosinY, a small fluorescent molecule that binds to chitosan polymers, for further microscopic analysis of Cu-sufficient and Cu-deficient *Cn* cells (Figs 4F and S2C and S2D). Consistent with the biochemical data, we observed decreased EosinY staining intensity in copper-starved *cbi1*Δ cells.

We also performed flow cytometry on CFW- and WGA-Alexa 488-stained cells to more precisely quantify the altered chitin/chitosan staining pattern in these strains (Figs 5A–5D and S2E and S2F). We directly compared WGA-Alexa 488 staining intensity to CFW staining intensity to assess chito-oligomer exposure relative to total cell wall chito-oligomer content. In copper-sufficient growth conditions, there was a small but statistically significant decrease in WGA-Alexa 488 staining intensity of the *cbi1*Δ cells compared to WT and complemented strains. However, we observed a notable increase in relative WGA staining in a sizable subpopulation of *cbi1*Δ cells ("High WGA", Figs 5C and 5D and S2E) during copper-starvation, consistent with the fluorescent microscopy results.

Upon infection, *Cn* has to react to and withstand a combination of abiotic and biotic stresses, including metal stress. To investigate whether the observed changes of the cell wall architecture in the *cbi1Δ* mutant are also induced under host-like stress conditions, we cultured WT, *cbi1*Δ, and *cbi1*$\Delta^{C\text{-}WT}$ cells for 24h in CO_2-indepedent medium (CIM) at 37˚C and performed microscopy and FACS analysis of CFW- and WGA-Alexa 488-stained cells (Fig 5E and 5F). Similar to *cbi1Δ* cells grown in copper-deficient YPD medium, we observed an increase in WGA-Alexa 488 staining signal in a significant subpopulation of *cbi1*Δ mutant cells after incubation in CIM.

One potential physiological consequence of aberrant *cbi1*Δ cell wall architecture is increased activation of host innate immune cells, as previously reported with other *Cn* strains

with increased chitin and chitosan exposure [34,35]. We co-incubated the fungal strains with murine bone marrow-derived macrophages (BMM), assessing TNF-α production as a marker of host immune cell activation. Macrophages exposed to copper-deficient *cbi1*Δ cells showed a statistically significant increase in TNF-α secretion compared to macrophages co-incubated with similarly treated WT or complemented strains (Fig 5G). No differences in TNF-α production were noted for macrophages incubated with any of these strains grown in the presence of copper. Together, these findings suggest that copper-deficient *cbi1Δ* cells not only have a decreased total cell wall chitin and chitosan content, but also that these polysaccharides are deposited in an aberrant manner within the cell wall leading to a higher degree of exposure in a manner that is detectable by host immune cells.

To explore the role of chitosan for modulating the resistance to copper stress, we assessed the growth effects during low and high copper stress for strains with mutations in either copper homeostasis or chitosan synthesis (Fig 5H and 5I). As previously described, we observed poor growth of the *cbi1*Δ and *ctr1*Δ strains during copper deficiency (Fig 5H). In line with previous findings, no sensitivity to copper starvation was observed for the *ctr4*Δ copper transporter mutant strain [36]. These results indicate that the Cbi1/Ctr1 complex can likely compensate for the loss of Ctr4, but that the Ctr4 transporter is not sufficient to maintain *Cn* growth during copper starvation in the absence of Ctr1. A slight reduction in growth was observed for the chitosan-deficient *chs3*Δ strain during copper starvation. Chs3 is responsible for the synthesis of most of the chitin destined to be converted to chitosan, suggesting that reductions in chitosan by varied mechanisms may affect the ability of *Cn to* withstand low copper stress. No growth phenotype was observed for the *cda2*Δ chitin deacetylase gene, indicating that the observed dysregulation of *CDA2* in the *cbi1*Δ background does not fully explain the *cbi1*Δ growth defect during copper deficiency.

To assess the role of cell wall chitin and chitosan in resistance to copper toxicity, we tested the *chs3*Δ and *cda2*Δ mutant strains for growth in the presence of increasing copper concentations (Fig 5I). The chitosan-deficient *chs3Δ* strain was more sensitive to high copper stress than the wild-type, and similar in its copper sensivity to strains with mutations in the *Cn* metallothionein genes *CMT1* and *CMT2* that mediate scavenging of excess copper. In contrast to *chs3*Δ, the *cda2*Δ strain, with a mutation in a single chitin deacetylase gene but relatively preserved cell wall chitosan levels, demonstrated increased resistance to toxic copper levels compared to WT. The *cbi1*Δ mutant displayed a similar copper resistance profile as the *cda2*Δ strain. This increased copper resistance was not shared with the *ctr1*Δ copper transporter mutant and and less apparent in the *ctr4*Δ mutant strain, suggesting that altered copper transport alone was not responsible for this phenotype. These findings suggest an unexpected new role for Cbi1 in modulating growth during high copper stress.

Cell wall changes in response to low copper stress lead altered caspofungin tolerance, melanin deposition and capsule architecture

Compared to many fungal pathogens, *C. neoformans* is relatively tolerant to caspofungin, an antifungal drug that inhibits β-glucan synthesis. However, *C. neoformans* strains with defects in chitosan production are more susceptible to this drug [37]. This observation is consistent with a conserved compensatory increase in cell wall chitin and chitosan among diverse fungi upon treatment with caspofungin [38,39]. Given the reduced cell wall chito-oligomer content in the copper-starved *cbi1Δ* mutant, we hypothesized that this strain would be more susceptible to caspofungin. Consistent with this hypothesis, we observed an 8-fold decrease in the effective inhibitory dose for 50% growth inhibition (ED_{50}) for caspofungin for the *cbi1*Δ mutant strain compared to the WT and reconstituted strains when incubated in copper-

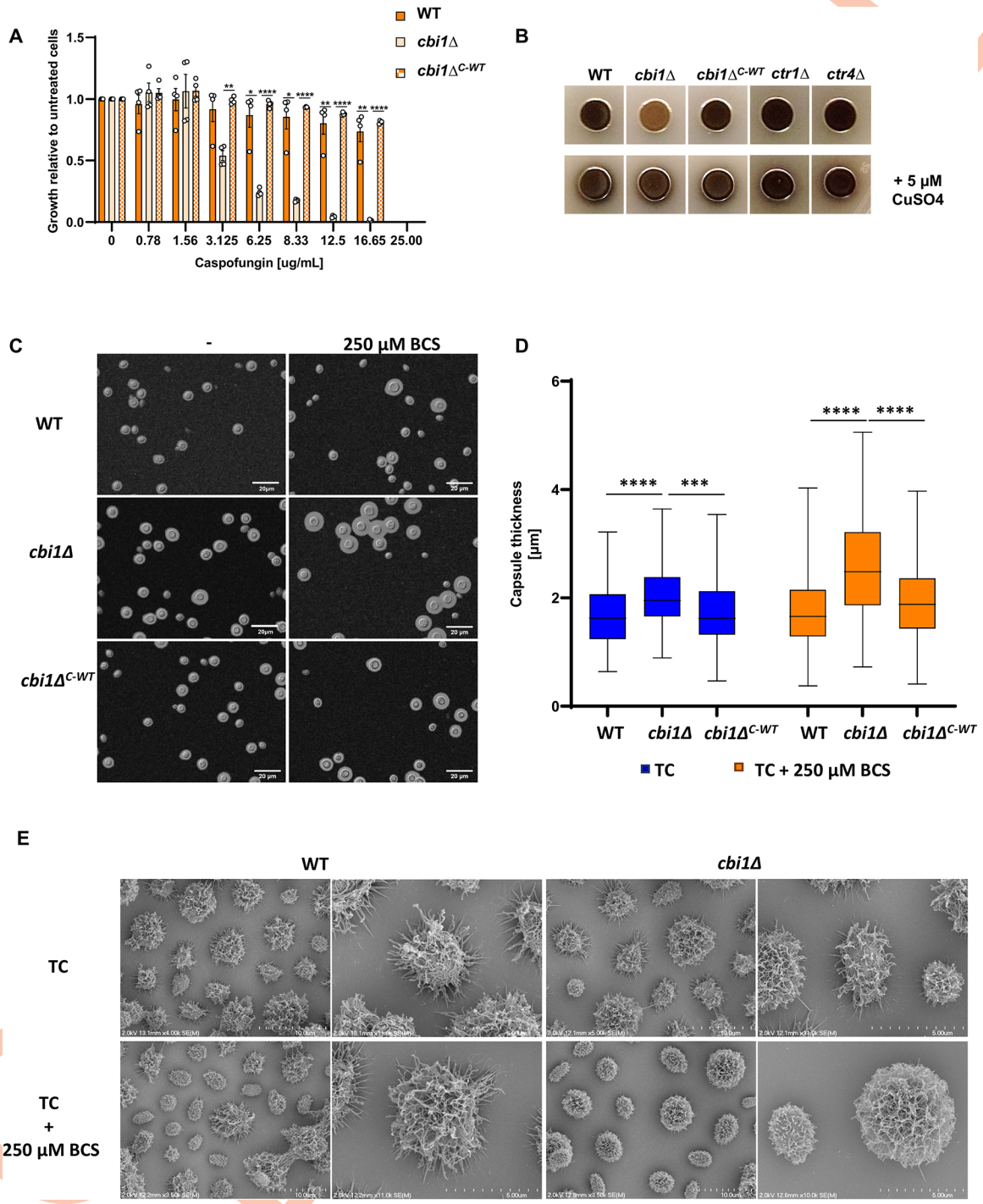

Fig 6. Cbi1 depletion and copper deficiency impacts cell wall-associated virulence phenotypes. (A) Minimal inhibitory concentration (MIC) analysis of caspofungin during copper deficiency. WT, *cbi1*Δ and *cbi1*$\Delta^{C\text{-}WT}$ strains were grown in 96-well liquid cultures in SC media supplemented with 100 μM BCS and were serial dilutions of caspofungin. OD_{600} was measured after 24h of growth at 30˚C and the OD_{600} of the non-treated condition was set to 1. Presented is the mean +/- SEM of 4 independent experiments. A 2-way ANOVA was performed from log transformed data using GraphPad Prism. **(B)** Melanization of WT, *cbi1*Δ, *ctr1*Δ and *ctr4*Δ cells in the absence and presence of 5 μM $CuSO_4$. Overnight cultures were harvested, washed 1x with PBS, diluted to OD_{600} 2.5 and spotted on to L-DOPA plates to induce melanin production. Shown are representative images from 3 independent experiments. **(C)** Analysis of capsule formation using India ink counter-staining of WT, *cbi1*Δ, and *cbi1*$\Delta^{C\text{-}WT}$ complemented cells. Indicated strains were grown for 3d in capsule inducing conditions in presence and absence of 250 μM BCS. Cell were harvest, resuspended in PBS, stained with India ink (1,1) and analyzed using DIC optics. Shown are representative images from 3 independent experiments. Scale bar 20 μm. **(D)**

Quantification of capsule size from India ink staining. Images taken were analyzed with imageJ/Fiji. A minimum of 170 cells of each strain were analyzed. Data are presented as box and whiskers diagram with indicated median and min/max capsule size measured for the indicated strains. A mixed effect analysis was performed using the log transformed data. **(E)** Scanning electron microscopy (SEM) analysis of WT and *cbi1*Δ cells after incubation in CO_2-independent medium for 3 days in absence and presence of 250 μM BCS.

https://doi.org/10.1371/journal.ppat.1010195.g006

deficient conditions (MIC_{50} *cbi1*Δ 3.1 μM) (Figs 6A and S2G). This suggests that the fungal cell wall mediates durable and adaptive cellular responses to copper availability that affect antifungal drug activity.

The cryptococcal capsule is composed of highly branching polysaccharides that are covalently attached to components of the outer surface of the cell wall, especially α-1,3 glucans [40]. The thickness of the capsule is induced during incubation conditions that mimic the host environment, including slightly alkaline pH and micronutrient limitation [11]. Strains with mutations in several chitin deacetylase genes, in particular with a *cda2* deletion, typically display enlarged capsules [22]. Similarly, the *cbi1*Δ mutant, in which *CDA2* levels are reduced, displayed more surface capsule, especially in copper limiting conditions (Fig 6C and 6D).

We performed scanning electron microscopic (SEM) analysis of WT and *cbi1*Δ cells after 3d of capsule induction in the absence and presence of 250 μM BCS (Fig 6E and 6F) to further analyze the role of Cbi1 in capsule architecture with a higher topographical resolution. Similar to capsule assessment by India ink counterstaining, we observed the most notable alterations in the capsular structure of the *cbi1*Δ strain during copper limitation. Under normal capsule-inducing conditions, both strains showed typical capsule architecture with a dense inner zone and a less dense outer layer consisting of extended capsule fibers [40]. However, when copper deficiency was induced by BCS supplementation, the *cbi1*Δ capsule displayed denser and more interconnected polysaccharide fibers compared to WT, with fewer freely extending individual capsule fibers.

Both copper limitation and cell wall alterations are important for the regulation of melanin, a cell wall-associated antioxidant pigment [24,30]. Melanin production itself is tightly linked to cellular copper levels since the rate-limiting phenoloxidase enzyme involved in melanin synthesis, laccase-1 (*Cn* Lac1), is functionally dependent on copper [41]. The *cbi1*Δ strain displayed defective melanin production on L-DOPA containing media (Fig 6B). The restoration of normal melanin production by the addition of 5 μM $CuSO_4$ is consistent with the known defects in copper acquisition in this strain [5]. We did not observe altered melanin production for the *ctr1*Δ or *ctr4*Δ strains, suggesting that the degree of intracellular copper limitation is greater in the absence of of the Cbi1 protein than in either of the single copper transporter mutants. Also, chitosan is required for the incoporation of melanin within the cell wall, and strains completely lacking chitosan display a "leaky melanin phenotype" in which melanin diffuses from the cell into the growth medium [22]. Even though depletion of Cbi1 affects cell wall chitosan levels during copper deficiency, we did not observe a leaky melanin phenotype. This is consistent with a reduction but not the complete absence of chitosan in the *cbi1*Δ strain. Together these results suggest that Cbi1-mediated cell wall remodeling and copper homeostasis affect the establishment of several cell wall-associated virulence factors.

Discussion

In these experiments we demonstrated an important interaction between copper homeostasis and the maintenance of fungal cell wall integrity. Deletion of either the Cuf1 copper-responsive transcription factor or the Cbi1 copper-binding cell surface protein renders *C. neoformans* more susceptible to cell wall stress. This central result suggests that copper homeostasis mechanisms affect the integrity of the fungal cell wall. In turn, we demonstrated that genes involved

in cell wall chitosan biosynthesis modulate resistance to copper stress. Furthermore, we characterized the biochemical and physiological changes that occur in the cryptococcal cell wall in response to low copper availability. These changes include a reduction in the amount of chitin and chitosan, two structurally related carbohydrates that are typically deeply embedded in the cell wall, as well as a greater exposure of the residual chito-oligomers on the *Cn* cell surface. Other cell wall-associated processes that were also altered in the *cbi1* mutant include an increased accumulation of surface capsule and a reduction in melanin, two mediators of virulence in this human fungal pathogen.

Copper regulation by the infected host is an important mechanism of immune response to invading pathogens. In contrast to the well-described "nutritional immunity" that primarily involves the sequestering of other essential micronutrients such as iron and zinc away from infecting microorganisms, the host regulation of copper involves a complex coordination of copper sequestion in certain tissues and the induction of very high copper levels in other sites [3,23,42,43]. In this way, microbial pathogens must be able to acquire sufficient copper for cell metabolism and energy production while simultanesously preventing the harmful effects of host-induced copper toxicity. In *C. neoformans*, the Cuf1 transcription factor controls this cellular response to both low and high copper concentrations [2,4]. In contrast, many other fungal species, both pathogens and nonpathogens, utilize distinct transcriptional regulators for each of these copper states. A genome-wide analysis identified many new and novel copper- and Cuf1-regulated genes, likely reflecting the wide range of copper concentrations encountered by this fungal pathogen in its varied environmental niches [4].

In response to high copper stress, microorganisms have developed multiple means of copper detoxification, including copper efflux systems as well as the induction of the copper-binding metallothionein proteins [2,43]. In *C. neoformans*, expression of the *CMT1* and *CMT2* metallothionein genes is controlled by Cuf1 in response to elevated copper levels, and these genes are required for fungal survival at sites of high copper exposure such as the host lung tissue [42]. Another reported defense mechanism against the effects caused by high copper stress is the up-regulation of the *ATM1* gene, required for transport of a Fe-S precursor into the cytosol to protect cytosolic Fe-S cluster proteins from mis-metalation caused by unbound, free Cu^{+} ions [44]. Recent reports have also demonstrated *Cn* proteomic responses to copper toxicity, including inhibition of protein translation and the induction of ubiquitin-mediated protein degradation [45]. Additionally, metabolic profiling of *Cn* during high copper stress demonstrated large changes in carbohydrate and amino acid metabolites [46]. In this study, we observed that the *CBI1* and *CDA2* genes, which are both regulated by Cuf1, are required for adaptive cell wall remodelling in response to copper stress, specifically by altering the cell wall chitin/chitosan layer.

Despite its toxicity, copper is essential for critical cellular processes, serving as a catalytic cofactor that drives iron uptake and distribution, mitochondrial cytochrome oxidase activity, and reactive oxygen (ROS) detoxification through the Cu/Zn superoxide dismutase (Sod1) [2]. Therefore, in response to low copper stress, microbes have evolved strategies to increase copper uptake efficiency and to direct copper to sites where it is most needed [2,47,48]. In *C. neoformans*, increased expression of the copper importer genes *CTR1* and *CTR4* and the *CBI1* gene represents an early response to copper limitation, an important adaption for fungal survival at sites of copper limitation [4,5,23,36]. A recent study demonstrated another copper sparing mechanism used by *C. neoformans* to adapt to copper limitation in which Cuf1 directs the transcriptional down-regulation of the copper-dependent superoxide dismutase *SOD1* gene and the simultaneous re-localization of the copper-independent Sod2 protein to maintain cellular antioxidant defense levels during copper limitation [49].

Our study explores a potential connection between copper homeostasis and the fungal cell wall. The modulations of copper resistance observed in different chitosan mutant strains provide preliminary evidence that regulation of cell wall composition and architecture could be a component of the fungal cell response to copper stress. Based on our findings, we hypothesize that the fungal cell wall could serve two functions relevant to copper homeostasis. First, under conditions of copper excess, cell wall carbohydrates could bind copper ions to prevent cytotoxic copper stress. Second, under conditions of copper deficiency, the cell wall could release bound copper to metal transporters for maintenance of cell homeostasis. Our data suggest that the Cbi1 protein could be one component of this copper acquisition process between the Ctr1 copper transporter and the fungal cell wall. *CBI1* and *CTR1* are among the *Cn* genes with the highest degree of regulation by the copper-sensing Cuf1 transcription factor in conditions of Cu depletion [4,5]. The Cbi1 and Ctr1 proteins interact both physically and genetically [5]. Accordingly, the *cbi1*Δ and *ctr1*Δ mutants display some similar phenotypes: poor growth in the presence of copper deprivation and cell wall stress.

However, the Cbi1 protein appears to have functions that are independent of simply participating in Ctr1-mediated copper transport into the cell. The *cbi1*Δ strain has a more severe, but copper-remediable, melanin defect than the *ctr1*Δ strain, suggesting a greater degree of intracellular copper limitation or altered copper acquisition. Moreover, only the *cbi1*Δ mutant, and not the *ctr1*Δ or *ctr4*Δ copper transporter mutants, displayed enhanced resistance to toxic copper levels. These results begin to suggest a new potential role for cell wall polysaccharides in adaptation to environmental changes. Since cell wall polysaccharides such as chitin and chitosan are known to avidly bind divalent metal ions such as Cu^{2+}, it is likely that their presence in the fungal cell wall serves to similarly bind copper encountered in the environment. Recent work with the model yeast *Pichia Pastoris* has established several cellular components involved in Cu^{2+} biopsorption. This study showed that in particular components within the *Pichia Pastoris* cell wall played an in important role in the biosorption process and demonstrated that several side groups found in proteins, polysaccharides and fatty acids are involved in Cu^{2+} adsorption [50]. Likewise, our copper titration experiments showed in the basidiomycete *C. neoformans* adsorption of copper from the environment in a dose dependent manner. Therefore, at higher levels of environmental copper, cell wall carbohydrate polymers such as chitosan might bind copper, protecting the cell body and membranes against the toxic effects of free Cu^{2+} ions. At lower levels of copper exposure, cell wall-associated Cu^{2+} ions might provide a readily accessible storage site for the copper transporter complexes.

The Cbi1 protein displays some degree of sequence similarity to proteins such as LPMOs that bind complex carbohydrate surfaces and promote further structural alterations by hydrolytic activity [51]. LPMOs have been best explored in the context of degradation of crystalline cellulose and chitin [52]. We have previously demonstrated that Cbi1 binds copper, but it lacks the redox activity that defines the LPMO class of enzymes [5,6]. Its copper-binding activity, and its physical association with the Ctr1 protein, suggest that Cbi1 might act as an intermediary to shuttle copper from the cell wall storage sites to the copper importer system. Our TEM data here support this model. In these images, the electron density of the chitin/chitosan cell wall layer remains unchanged in the *cbi1*Δ mutant during extracellular copper starvation. In contrast, the electron density of this layer in WT cells decreases during copper starvation. The exact species of the high electron dense molecule shuffled in response to copper limitation still has to be defined in future studies. Nevertheless, the observed pattern is in agreement with our model postulating a cellular import of copper ions from the cell wall mediated in part by Cbi1.

Here we have demonstrated that the absence of Cbi1 is also associated with transcriptional changes in cell wall genes, and that these transcriptional changes result in functional

consequences for the *Cn* cell wall. These changes include reduced levels of chitin and chitosan as well as altered cell wall architecture, especially in the presence of copper limitation. As a result, cell wall-associated virulence factors are altered in function, resulting in changes in the interaction with host immune cells. The specific activity of the Cbi1 protein has yet to be determined. Also, it is not yet clear whether the cell wall changes in the *cbi1*Δ strain are directly related to Cbi1 function or whether they represent compensatory cellular changes in response to stress. This type of cell wall adaptation to cell stress is commonly observed in other conditions [53]. For example, cell wall chitin levels are increased in the human fungal pathogens *Aspergillus fumigatus* and *C. neoformans* during treatment with the beta-glucan synthase inhibitor capofungin [37]. Blunting this adaptive cell wall chitin response renders these cell more susceptible to the activity of this antifungal agent. Similarly, we demonstrated here that the *cbi1*Δ mutation, and its downstream defective cell wall response, results in a similar degree of enhanced caspofungin susceptibility as strains with mutations in chitin synthesis genes themselves [37].

Our observations of significant reductions in cell wall chitosan in the copper-starved *cbi1*Δ strain together with the direct regulation of one of the chitin deactylases *CDA2* by the copper responsive transcription factor Cuf1 [4], suggest that this cell wall polymer may contribute to copper homeostasis. In contrast to many ascomycete fungal pathogens, *C. neoformans* contains much more chitosan in the inner chito-oligomer layers of the cell wall [8]. Chitosan is a relatively de-acetylated form of chitin. Both chitin and chitosan exist in varying sizes, the polymer length determined by both endogenous and exogenous synthases and chitinases. In fact, the size of fungal chitin and chitosan molecules, as well as their relative degrees of acetylation/deacetylation, determine their immunogenicity [54,55]. Therefore, both host and microbe possess intricate means to regulate chito-oligomer molecular size and acetylation status [8,13,56].

In *C. neoformans*, four putative chitin deacetylases contribute to the conversion of chitin to chitosan: Cda1, Cda2, Cda3, and Fpd1. Prior mutational analysis revealed that a *Cn cda1,2,3* triple mutant is devoid of most measurable cell wall chitosan during vegetative growth [22]. Although the Fpd1 enzyme is not required for chitosan conversion from chitin under normal growth conditions, it may contribute to the further deacetylation of pre-formed chitosan [57]. Consistent with the decrease of cell wall chitosan in the *cbi1*Δ mutant, we identified two of the four chitin deacetylase genes, *CDA2* and *FPD1*, to be down-regulated in copper-deficient *cbi1Δ* cells. Hence, Cda2 and Fpd1 may be involved in regulating cell wall chitosan levels in response to cellular copper levels. Therefore, Fpd1 together with Cda2 could potentially be involved in modulating the deacetylation ratio of chitosan molecules, and by doing so modulating the copper binding capacity of the aggregate cell wall sugar polymers in response to changing copper levels.

In summary, we have defined cell wall changes that modulate stress adaptation of a fungal pathogen during conditions associated with human infection, including both high and low copper levels. We have further proposed a model in which the fungal cell wall might serve as a copper-binding organelle to prevent excessive intracellular accumulation during copper toxicity as well as a site for copper delivery to copper transporters during low copper states. Furthermore, we have defined cellular roles for a unique copper-binding protein that might serve to mediate copper transfer between the fungal cell wall and copper import proteins.

Material and methods

Ethics statement

All animal experiments in this manuscript were approved by the Duke University Institutional Animal Care and Use Committee (IACUC) (protocol #A102-20-05). Mice were handled according to IACUC guidelines.

Strains, media and growth conditions

Cryptococcus neoformans strains used in this study are shown in **S2 Table.** All strains were generated in the *C. neoformans var. grubii H99* background. For strain creation, DNA was introduced into *C. neoformans* by biolistic transformation [58]. Yeast extract (2%)-peptone (1%)-dextrose (2%) (YPD) medium supplemented with 2% agar and 100 μg ml-1 of nourseothricin (NAT), 200 μg ml-1 of neomycin (G418) or 200 μg ml-1 of hygromycin B (HYG) was used for colony selection after biolistic transformation. Cloning strategies as well as plasmids and oligos used for creation of *Cryptococcus* transformation constructs are described in **S3 and S4 Tables** Transformants were screened by PCR and Southern blot for intended mutations. Cbi1-HA expression among relevant transformants was confirmed by western blot.

Strains were cultivated in either synthetic complete (SC) medium (MP Biomedicals) or YPD at 30˚C. To induce Cu sufficiency or deficiency, media was supplemented with indicated concentrations of $CuSO_4$ or the Cu^+ chelator bathocuproine disulfonate (BCS), respectively. Alternatively, to BCS supplementation, strains were cultivated in Yeast extract-peptone medium supplemented with 3% Glycerol and 2% Ethanol (YPEG). For galactose-regulated expression induction, SC+2% Galactose (SC-Gal) or SC+2% Glucose (SC-Glu) was used and supplemented as indicated. To analyze cell wall associated phenotypes, caffeine (0.5 mg/ mL), NaCl (1.5 M), SDS (0.01%), Congo red (0.5%) and Calcofluor White (1.5 mg/mL) were added to SC medium supplemented with $CuSO_4$ or BCS as indicated. For growth phenotype analysis on solid medium plates, a 6-fold serial dilution, starting at OD_{600} 0.25, of strains was spotted and incubated for indicated time and temperature. For assessment of melanization, overnight cultures in YPD were washed once in PBS and resuspended in PBS to OD_{600} 2.5. Next, 5 to 10 μL of the resuspended culture were spotted onto L-3,4-dihydroxyphenylalanine (L-DOPA) media (7.6 mM L-asparagine monohydrate, 5.6 mM glucose, 22 mM KH2PO4, 1 mM MgSO4.7H2O, 0.5 mM L-DOPA, 0.3 μM thiamine-HCl, 20 nM biotin, pH 5.6). L-DOPA plates were incubated at 30˚C for 2 days. To induce capsule, strains were incubated in CO2-independent tissue culture medium supplemented as indicated (TC, Gibco) for 72 hours with shaking at 37˚C, followed by staining with India Ink or fixation for scanning electron microscopy (SEM).

RNA isolation and qRT-PCR

For *ROM2* transcript analysis *C. neoformans* overnight cultures grown in synthetic complete (SC) medium (MP Biomedicals) were diluted to OD_{600} 0.3, and cultures were supplemented and cultivated as indicated. For cell wall synthesis genes transcript analysis and copper status analysis, *C. neoformans* overnight cultures grown in YPD medium were diluted to OD_{600} 0.05, supplemented as indicated and cultivated for 24h at 30˚C. For RNA extraction, cells were cultivated as indicated. Cultures were harvested, washed 1x with PBS and flash frozen on dry ice, followed by lyophilization. RNA was extracted using the RNeasy Plant Mini Kit (Qiagen) with optional on-column DNAse digestion. cDNA for real time-PCR (RT-PCR) was prepared using the Iscript cDNA synthesis kit (Biorad). For RT-PCR, cDNA was diluted 1:5 in RNase-free water, added to ITAQ Universal SYBR Green Supermix (Bio-Rad) per protocol

instructions and analyzed on a CFX384 C1000 ThermoCycler (BioRad, ROM2 analysis and Cu status analysis). For analysis of cell wall transcripts, the diluted RNA was mixed with the PowerUP SYBR Green Master mix (applied biosystems) per protocol instruction and analyzed on a QuantStudio 6 Flex (applied biosystems). Oligos used for qRT-PCR analysis are shown in **S4 Table.** C_T values were determined using the included CFX Maestro software (BioRad) or the QuantStudio 6 Flex, respectively. Gene expression values were normalized to the housekeeping gene *GAPDH* and expression fold changes determined by the $\Delta\Delta C_T$ method. For all qRT-PCR studies, a minimum of 3 independent biological replicates were used for the analysis of mRNA expression changes.

Inductively coupled plasma mass spectrometry (ICP-MS)

Cell associated metals (Fe and Cu) were quantified from lyophilized *Cn* cells. In short, yeast cells were treated as indicated, spun down and washed 2x with ICP-MS grade water. In the last wash step, cell were counted, spun down and lyophilized. Samples were digested in 300 uL 50% ICP-MS grade Nitric Acid for 1h, at 90˚C and cooled down overnight at RT. Metal content was analyzed by ICP-MS at the Oregon Health Sciences University Elemental Analysis Shared Resource using an Agilent 7700X ICP-MS as published previously [49].

Anodic stripping voltammetry (ASV)

The ASV experiment was performed with live cells. Cells were cultivated in copper deficient conditions (YPD + 250 μM BCS) for 24h at 30˚C to remove loosely bound copper on the surface of the *Cn* cells. Prior to analysis, cells were harvested and washed 3x with 25 mL PBS and resuspended in PBS. Cells were counted twice and normalized to either 10^5 cells/ mL or 10^7 cells/mL (in PBS) for analysis. Copper concentration between 250 nM to 1000nM were titrated stepwise into 20 mL cell suspensions and copper adsorption after each titration step was measured using a static mercury drop electrode (663VA Stand and PGSTAT 128N potentiostat, Metrohm-Autolab, drop size 2), an Ag/AgCl, KCl (3 M) reference electrode with a 3M KCl salt bridge, and a glassy carbon counter electrode. Samples were initially purged with highpurity N2 (5.0, Airgas) for 180 s. ASV stripping peak currents were measured after a deposition time of 90s at -1.2 V. After an equilibration time of 5 s, the potential was ramped from −1.2V to 0V using a square wave voltammetry (scan rate 0.12Vs−1; amplitude 0.02V; frequency 60Hz). For analysis the measured curve was smoothed and the peak height at E = -0.12V was determined. For each titration experiment, the peak height was plotted against titrated Cu concentration and a linear regression was performed to calculate the slope (measured current/ nM Cu).

Liquid growth assays

All liquid growth analysis were performed in 96 well plates. For the growth analysis in YPEG in the presence of the surface stressor SDS, overnight cultures (YPD, 30˚C), were harvested and washed 1x with YPEG and then normalized to OD_{600} 2.0 (in YPEG). Growth media was supplemented as indicated and filled into 96 well plate (195 μL each well). Wells were inoculated with 5 μL of indicated strain (final OD_{600} = 0.05). Plates were covered with a semipermeable membrane (Breathe-Easy, Diversified Biotech) and incubated at 30˚C with shaking at 1150 rpm in a Finstruments shaker instrument. Growth graphs of the indicated strains at the conditions analyzed were generated by plotting the OD_{600} readings normalized to WT-YPEG growth at the 24 h time point. Three biological replicates were performed.

For minimal inhibitory concentration analysis (MIC), overnight cultures (SC, 30˚C), were harvested and washed 1x with PBS and then set to OD_{600} 0.25 (in PBS) and stored on ice until further usage. 2x concentrated working stocks of caspofungin were prepared in SC medium

(final concentration in assay ranged 100 to 0.78 μg/mL). Cells were diluted 1:100 in either SC or SC+200 μM BCS (final concentration in assay 100 μM BCS). In 96 well plate, 100 μL of diluted cells were mixed with 100 μL of 2x concentrated caspofungin stocks. The plate was covered with a semipermeable membrane (Breathe-Easy, Diversified Biotech) and incubated at 30˚C with shaking at 1150 rpm in a Finstruments shaker instrument for 24h. Growth graphs of the indicated strains at the conditions analyzed were generated by calculating the relative growth of the drug-treated condition in relation to the untreated condition (drug-treated OD600/untreated OD600). Four biological replicates were performed.

Transmission electron microscopy (TEM)

Overnight cultures (YPD, 30˚C) were harvested and washed 1x with YPD. Indicated strains were inoculated to an OD_{600} of 0.05 in 50 mL YPD + 10 μM $CuSO_4$ (= Cu sufficiency) or 250 μM BCS (= Cu deficiency) and cultivated for 24h at 30˚C. In the following day, 50 to 100 μL of the culture were harvested and washed 1x with PBS. Next, cells were pelleted and overlayed with fixative (4% formaldehyde, 2% Glutaraldehyde in PBS) and incubated for 4h at RT. Then, fixative was removed, and the sample was washed twice with 1x PBS, with a 10 minute incubation time at RT in between wash steps. After last washing step, the PBS was removed and 1% OsO_4 was added to the sample to complete cover. The tube was sealed and incubated for 1h at RT in the dark. Then the OsO_4 was removed, and the sample rinsed with 1x PBS, 2 times for at least 10 minutes each time (RT). After last PBS rinse, residual PBS was removed and the sample was rinsed with 0.1N acetate buffer, 1 time at least 10 minutes each time (RT). The acetate buffer was removed, and the sample was stained with 0.5% uranyl acetate (UA) for one hour, RT. Once staining was complete, the uranyl acetate was removed and the sample rinsed with 0.1N acetate buffer, 2 times at least 10 minutes each time. In the next steps the samples were dehydrated in several ethanol incubation steps by rinsing twice, at least 10 minutes each time, with 30% Ethanol, 50% Ethanol, 70% Ethanol and 90% Ethanol. Finally, the sample were rinsed 3 times, at least 10 minutes each time, with 100% Ethanol.

Once the dehydration was complete, ethanol was removed and the dehydrated sample was embedded into resin (53,5% (w/v) resin, 20.5% (w/v) DDSA, 26% (w/v) NMA, 1.4% (v/v) DMP-30). The sample were incubated in resin mix at RT overnight. The following day, samples were incubated at 50–60˚C for 10 minutes, the old resin mix was replaced by freshly made resin mix and incubated for 10 mins at RT, followed by 10 minutes at at 50–60˚C. This resin wash step was repeated one more time, followed by a 48h incubation at 50–60˚C. The embedded samples were cut into 70nm thick sections on an Ultracut microtome and placed on TEM grids. The sections were counterstained with uranyl acetate and lead citrate and then imaged on an FEI Technai G2 Twin transmission electron microscope. Cell wall thickness was measured using ImageJ (Cu sufficient WT: 8 cells, Cu deficient WT: 7 cells, Cu sufficient *cbi1Δ*: 14 cells and Cu deficient *cbi1Δ*: 10 cells). The staining contrast in the cell wall was measured using Image J gray scale measurement tool.

Scanning electron microscopy (SEM)

Overnight cultures (YPD, 30˚C) were harvested and washed 1x with PBS. Indicated strains were inoculated to an OD_{600} of 0.1 in 25 mL CO_2-independent medium (Gibco) or 25 mL CO_2-independent medium supplemented with 250 μM BCS and cultivated for 3d at 37˚C. 5 mL of each culture were harvested, checked for capsule formation by India ink stain and washed 3x with PBS (without calcium and magnesium). Cells were fixed for 1h at RT with 2.5% glutaraldehyde in PBS, washed 3 times with PBS and checked for intact capsule by india ink staining. Then, cells were mounted onto poly-L-lysine-coated coverslips (Neuvitro, 12mm,

#1 thickness coverlsips) and incubated for 20 min at RT. After mounting, cells were sequentially dehydrated in several ethanol washes (1x 30%, 1X 50%, 1X 70%, each 5 min RT, followed by 1x 95% and 2x 100%, 10 min RT). After dehydration mounted cells were stored in 100% ethanol until the critical point drying. Cell samples were critical point dried with a Tousimis 931 critical point dryer (Rockville, Maryland) and coated with gold-palladium using a Cressington 108 sputter-coater (Watford, United Kingdom). Samples were mounted and imaged on a Hitachi S-4700 scanning electron microscope (Tokyo, Japan).

Cell wall isolation and analysis

Overnight cultures (YPD, 30˚C) were harvested and washed 1x with YPD. Indicated strains were inoculated to an OD_{600} of 0.05 in 50 mL YPD + 10 μM $CuSO_4$ (= Cu sufficiency) or 250 μM BCS (= Cu deficiency) and cultivated for 24h at 30˚C. The following day, 10 to 25 mL of the cells were harvested and washed twice with dH_2O. In the last wash step, cells were counted, spun down and lyophilized. Chitin and chitosan levels were quantified from lyophilized yeast using a modified MBTH (3-methyl-benzothiazolinone hydrazine hydrochloride) method as previously described [13]. β-glucan was quantified using the megazyme yeast β-glucan kit. In short lyophilized yeast were milled using glass beads, resuspended in 800 μL 2 M KOH and transferred into a new 12 ml reaction tube and stirred for 30 mins in an ice water bath. Then, 3.2 mL of 1.2 M sodium acetate pH 8.3 and 40 μL glucazyme was added and the sample stirred for 2 min. The sample was transferred to a 15 mL screw cap tube and incubated ON at 40˚C in a water bath. The next day, 10 mL dH_2O was added to the samples, mixed thoroughly and centrifuged for 10 mins at 3000 rpm. Then, 100 μL of the supernatant was mixed with GOPOD reagent and incubated for 20 mins at 40˚C in a water bath. 2 x200 μL of each sample were transferred into a 96 well plate and read (against reagent blank) at 510 nm. A standard curve was prepared using the manufacturer's supplied D-glucose standard solution and mg glucose was calculated using equation provided by manufacturer. Measured values were normalized by cell count.

Cell wall staining and flow cytometry

Prior to analysis cells were treated as indicated. To visualize chitin, cells were harvested and stained with 100 μg/ml Alexa488-conjugated wheat germ agglutinin (WGA, Molecular Probes) for 35 minutes in the dark, RT, followed by 25 μg/ml calcofluor white (CFW, Fluka Analytical) for 10 minutes, RT. After staining, cells were washed 2x with PBS and were resuspended in 20–50 μL PBS for microscopic analysis. Alexa488-WGA was imaged using a GFP filter and CFW was imaged using a DAPI filter. For flow cytometry fixed or live cells were measured. For Fixation, cells were harvested and washed and then incubated for 5 mins in 3.5% Formaldehyde at RT. Cells were Alexa488-WGA and CFW stained as previously described, washed 2x with PBS and set to 10^6 cells (in 1 mL PBS). Alexa488-WGA stained cells were analyzed using a 488 nm laser and CFW cells were analyzed using a 405 nm laser. The FACS analysis was performed at the Duke Cancer Institute Flow Cytometry Shared Resource using a BD FACSCanto II flow cytometer. Data was analyzed using FlowJo v10.1 software (FlowJo, LLC). For analysis only single cells were used (gated using the FSC/SSC plot). For chitin exposure analysis cells were gated in the CFW intensity/ Alexa488-WGA intensity scatter plot. Additional histograms with mean fluorescence intensity (MFI) on the x-axis and cell counts on the y-axis were created. Unstained cells were used as negative controls.

To visualize chitosan, cells were treated as indicated, harvested and washed 2x with McIlvaine's buffer (0.2 M Na2HPO4, 0.1 M citric acid, pH 6.0). Then, cells were stained using 500 μL of 300 μg/ml Eosin Y in McIlvaine's buffer for 10 minutes at room temperature in the

dark. Cells were then washed 2x with McIlvaine's buffer and resuspended in 20–50 μL McIlvaine's buffer. Cells were visualized using a GFP filter.

Microscopic quantification

Differential interference microscopy (DIC) and fluorescent images were visualized with a Zeiss Axio Imager fluorescence microscope (64X objectives). Images were taken with an AxioCam MRm digital camera with ZEN Pro software (Zeiss). The same exposure time was used to image all strains analyzed. Images were analyzed using ImageJ/Fiji software. Gray scale values were measured and normalized towards cell count. The intensity of the control strain (= Cu sufficient WT) was set to 1. Results are reported as relative fluorescence intensity +/- standard error of the means.

Cells sizes were measured using the ImageJ measurement tool. Capsule thickness was calculated using the equation:

$$capsule\ thickness = \frac{(cell\ diameter\ including\ capsule - cell\ body\ diameter)}{2}$$

Generation of bone marrow derived macrophages

Murine bone marrow cells were isolated from A/J mice and prepared as previously described [34]. Briefly, femurs and tibias were isolated from mice. Each bone was flushed with 5 to 10 ml cold PBS using a 27½ gauge needle. Red blood cells were lysed in 1x RBC lysis buffer (0.15 M NH_4Cl, 1 mM $NaHCO_3$, pH 7.4) and cells were resuspended in 1x Dulbecco's modified Eagle's medium (DMEM; + 4.5 g/L D-Glucose, + L-Glutamine, +110 mg/L sodium pyruvate) with 1 U/ml pencillin/streptomycin. Bone marrow cells were cryopreserved in 90% FBS/10% endotoxin-free DMSO at a concentration of 1 x 10^7 cells/ml.

BMMs were differentiated in BMM medium (1x Dulbecco's modified Eagle's medium [DMEM; + 4.5 g/L D-Glucose, + L-Glutamine, +110 mg/L sodium pyruvate], 10% fetal bovine serum [FBS; non-heat inactivated], 1 U/ml penicillin/streptomycin) with 3 ng/ml recombinant mouse GM-CSF (rGM-CSF; R&D Systems or BioLegend)) at a concentration of 2.5 x 10^5 cells/ml in 150 x 15 mm petri plates at 37˚C with 5% CO_2. The media was refreshed every 3–4 days and the cells were harvested after ~7d or when confluency was achieved.

Macrophage co-incubation and TNF-α quantification

Prior to co-incubation, overnight cultures of *C. neoformans* strains (YPD, 30˚C) were harvested and washed 1x with YPD. Indicated strains were inoculated to an OD_{600} of 0.05 in 50 mL YPD + 10 μM $CuSO_4$ (= Cu sufficiency) or 250 μM BCS (= Cu deficiency) and cultivated for 24h at 30˚C. To prepare BMMs for the co-incubation assay, BMMs were counted (by hemocytometer, with Trypan blue to discount dead cells), plated in BMM medium in 96-well plates at a concentration of 5 x 10^4 cells/well and incubated at 37˚C with 5% CO_2 overnight. The next day C. *neoformans* cells were washed 2x with PBS, counted, and added to BMMs containing 96-well plates at a concentration of 5 x 10^5 fungal cells per well (10:1 *C. neoformans* cells:BMMs). Co-cultures were incubated for 6h at 37˚C with 5% CO_2. Supernatants were collected and stored at -80˚C until analysis. Secreted TNF-α was quantified in supernatants by enzyme-linked immunosorbent assay (ELISA; BioLegend).

Statistical analysis

All data error bars represent statistical errors of the means (SEM) of results from a number of biological replicates (N), as indicated in figure legends. Before statistical analysis was conducted, data from all experiments was log transformed for comparison of proportions. Statistical analysis was performed with GraphPad Prism software v9. The statistical tests chosen for each experiment and their results (i.e., p values) are indicated in figure legends. Asterisks in figures correspond to statistical significance as follows: ****, $P < 0.0001$; ***, $P = 0.0001$ to $P < 0.001$; **, $P = 0.001$ to $P < 0.01$; *, $P = 0.01$ to $P < 0.05$; ns (not significant), $P > 0.05$.

Supporting information

S1 Table. *C. neoformans* genes with proposed function in cell wall remodelling or carbohydrate synthesis identified by Garcia-Santamarina *et al.* to be transcriptionally regulated by copper and Cuf1 [4]. Shown is the Gene identifier, predicted gene product, and the $\log_2$ fold change in high Cu-treated WT versus low Cu-treated WT cells (log2FC WT Cu/BCS). Cuf1-Flag promoter binding is indicated as follows: N = No binding, Cu = Binding during high copper stress, BCS = Binding during low copper stress, Cu and BCS = Binding during both copper stress conditions.
(TIF)

S2 Table. Yeast strains used in this study.
(TIF)

S3 Table. Plasmids used in this study.
(TIF)

S4 Table. Oligonucleotides used in this study.
(TIF)

S1 Fig. (A-B) qRT-PCR analysis of the *ROM20 and CRZ1* transcript level in indicated strains during high copper (A) and low copper (B) stress. For the high copper condition, the WT, *cuf1*Δ and Cuf1-Flag complemented *cuf1*Δ^C strains were inoculated to OD_{600} 0.3 in SC supplemented with 1 mM $CuSO_4$ and cultivated for 1h at 30˚C. To induce low copper conditions, indicated strains were inoculated to OD_{600} 0.3 in SC supplemented with 1 mM BCS and cultivated for 6h at 30˚C. For comparison the WT transcript levels at each condition were set to 1. Presented is the mean +/- SEM of the relative transcript levels of 4 biological replicates. A 2-way ANOVA was performed using GraphPad Prism from log transformed data. **(C)** Growth analysis in presence of cell wall/ surface stressors. The spotting assay was performed on SC supplemented with indicated amounts of cell wall and cell surface stressors. Indicated strains were grown overnight in SC at 30˚C. Cells were diluted to OD_{600} of 0.25 and a serial 1:10 dilution was spotted on to media plates. Plates were incubated at 30˚C for 2-4d. This figure shows a representative image from 3 independent spotting experiments. **(D)** Growth rate of copper sufficient or deficient WT and *cbi1Δ* cells. Cells were incubated in YPD supplemented with 10 μM $CuSO_4$ (Cu sufficiency) or with 250 μM BCS (Cu deficiency) for 24h at 30˚C. Growth was measured through $0D_{600}$. Presented is the average +/- SEM of 5 biological replicates. **(E)** Colony forming unit (CFU) analysis of copper sufficient or deficient WT and *cbi1Δ* cells. Cells were treated as described in (B). After 24h of growth, cells were diluted to OD_{600} 1. 200 μL of a serial 1:1000 dilution were plated onto YPD plates and colonies were counted after 3d of incubation at 30˚C. The CFU of copper sufficient WT was set to 100%. Presented is the average +/- SEM of the relative CFU (as compared to copper sufficient WT) from 4 biological replicates. **(F)** qRT-PCR analysis using *CMT1* and *CTR4* as indicator for Cu toxicity or deficiency.

Indicated cells were cultivated as described in (B) and used for RNA extraction, followed by cDNA synthesis. Presented is $\Delta\Delta C_T$ of copper deficiency: copper sufficiency. The average +/- SEM from 3 biological replicates is shown. **(G)** Representative copper titration curves. Indicated strains were grown under Cu starvation (YPD + 250 μM BCS) for 24h at 30˚C. Copper was titrated in 250 nM steps into 20 mL cell suspension of indicated concentration or PBS (= control). The measured curves were smoothed using the NOVA softaware and potential with resulting current was exported. Curves were plotted using Graph Pad.
(TIF)

S2 Fig. **(A)** β-glucan quantification of copper sufficient and copper deficient wt, *cbi1*Δ and *cbi1*$\Delta^{C\text{-}WT}$ complemented cells. Strains were incubated for 24h in YPD+ 10 uM CuSO4 (Cu sufficiency) or YPD +250 uM BCS (Cu deficiency) and then harvested, cell counted and lyophilized. The Megazyme yeast b-glucan kit was used for quantification of b-glucan from lyophilized cells. Values are shown in ug Glucose / 10^7 cells. Presented is the average +/- SEM of 3 biological replicates. **(B)** Calcofluor white (CFW) and wheat germ agglutin (WGA)-Alexa 488 staining for chitin of copper sufficient or deficient WT, *cbi1*Δ and and Cbi1 WT complemented *cbi1*Δ (*cbi1*$\Delta^{C\text{-}WT}$) cells. Strains were cultivated as described in (A). Shown is the mean +/- SEM of the relative CFW intensity from 3 independent experiments. The CFW intensities were measured with ImageJ/Fiji and normalized to cell count. Shown is the relative CFW intensity (copper sufficient WT set to 1). A 1-way ANOVA was performed using GraphPad Prism from log transformed data. **(C)** EosinY staining for chitosan of copper sufficient and deficient WT, *cbi1*Δ and *cbi1*$\Delta^{C\text{-}WT}$ complemented cells. Strains were cultivated as described in (A), followed by EosinY staining. Shown are representative images for 2 two independent experiments. Five independent treatments and stainings were performed. **(D)** Relative EosinY intensity from 5 independent experiments. The EosinY intensities were measure with ImageJ/Fiji and normalized to cell count. Shown is mean +/- SEM of the relative EosinY intensity (copper sufficient WT set to 1). A 1-way ANOVA was performed using GraphPad Prism from log transformed data. **(E-F)** FACS analysis of CFW and WGA-Alexa 488 stained cells. WT, *cbi1*Δ and *cbi1*$\Delta^{C\text{-}WT}$ complemented cells were cultivated as described in (A) **(E)** WGA-Alexa 488 staining histogram representation of the FACS analysis depicted in Fig 3. **(F)** CFW-staining histogram representation of FACS analysis depicted in Fig 3. **(G)** Minimal inhibitory concentration (MIC) analysis of Caspofungin during copper sufficiency. WT, *cbi1*Δ and *cbi1*$\Delta^{C\text{-}WT}$ complemented cells were grown in 96-well liquid cultures in SC media supplemented with 0 to 100 ug/mL Caspofungin. OD_{600} were measured after 24h growth at 30˚C and the OD_{600} of the non-treated condition was set to 1. Presented is the mean +/- SEM of 4 independent experiments.
(TIF)

Acknowledgments

We thank the Duke Cancer Institute for the use of the Flow Cytometry Shared Resource. The Transmission electron microscopy was performed in part at the Duke University Shared Materials Instrumentation Facility (SMIF), a member of the North Carolina Research Triangle Nanotechnology Network (RTNN). Scanning electron microscopy was performed at the Chapel Hill Analytical and Nanofabrication Laboratory, CHANL, a member of the North Carolina Research Triangle Nanotechnology Network, RTNN. ICP-MS measurements were performed in the OHSU Elemental Analysis Shared Resource. We thank Dr. Aaron D. Smith for insightful discussions of the data and proposed model.

Author Contributions

Conceptualization: Corinna Probst, J. Andrew Alspaugh.

Data curation: Martina Ralle.

Formal analysis: Corinna Probst.

Funding acquisition: Dennis J. Thiele, J. Andrew Alspaugh.

Investigation: Corinna Probst, Sarela Garcia-Santamarina, Jacob T. Brooks, Inge Van Der Kloet, Oliver Baars.

Methodology: Corinna Probst, Sarela Garcia-Santamarina, Jacob T. Brooks, Oliver Baars, Martina Ralle.

Project administration: Inge Van Der Kloet.

Resources: Dennis J. Thiele.

Supervision: Oliver Baars, J. Andrew Alspaugh.

Validation: Inge Van Der Kloet.

Writing – original draft: Corinna Probst, J. Andrew Alspaugh.

Writing – review & editing: Corinna Probst, Sarela Garcia-Santamarina, Jacob T. Brooks, Oliver Baars, Martina Ralle, Dennis J. Thiele, J. Andrew Alspaugh.

References

1. Bleackley MR, MacGillivray RTA. Transition metal homeostasis: from yeast to human disease. BioMetals. 2011; 24(5):785–809. https://doi.org/10.1007/s10534-011-9451-4 PMID: 21479832
2. Smith AD, Logeman BL, Thiele DJ. Copper Acquisition and Utilization in Fungi. Annu Rev Microbiol. 2017; 71:597–623. Epub 2017/09/10. https://doi.org/10.1146/annurev-micro-030117-020444 PMID: 28886682
3. Hood MI, Skaar EP. Nutritional immunity: transition metals at the pathogen-host interface. Nat Rev Microbiol. 2012; 10(8):525–37. Epub 2012/07/17. https://doi.org/10.1038/nrmicro2836 PMID: 22796883
4. Garcia-Santamarina S, Festa RA, Smith AD, Yu CH, Probst C, Ding C, et al. Genome-wide analysis of the regulation of Cu metabolism in *Cryptococcus neoformans*. Mol Microbiol. 2018; 108(5):473–94. Epub 2018/04/03. https://doi.org/10.1111/mmi.13960 PMID: 29608794
5. Garcia-Santamarina S, Probst C, Festa RA, Ding C, Smith AD, Conklin SE, et al. A lytic polysaccharide monooxygenase-like protein functions in fungal copper import and meningitis. Nature Chemical Biology. 2020; 16(3):337–44. https://doi.org/10.1038/s41589-019-0437-9 PMID: 31932719
6. Brander S, Horvath I, Ipsen JO, Peciulyte A, Olsson L, Hernandez-Rollan C, et al. Biochemical evidence of both copper chelation and oxygenase activity at the histidine brace. Sci Rep. 2020; 10(1):16369. Epub 2020/10/03. https://doi.org/10.1038/s41598-020-73266-y PMID: 33004835
7. Labourel A, Frandsen KEH, Zhang F, Brouilly N, Grisel S, Haon M, et al. A fungal family of lytic polysaccharide monooxygenase-like copper proteins. Nature Chemical Biology. 2020; 16(3):345–50. https://doi.org/10.1038/s41589-019-0438-8 PMID: 31932718
8. Garcia-Rubio R, de Oliveira HC, Rivera J, Trevijano-Contador N. The Fungal Cell Wall: *Candida*, *Cryptococcus*, and *Aspergillus* Species. Front Microbiol. 2019; 10:2993. Epub 2020/01/30. https://doi.org/10.3389/fmicb.2019.02993 PMID: 31993032
9. Hopke A, Brown AJP, Hall RA, Wheeler RT. Dynamic Fungal Cell Wall Architecture in Stress Adaptation and Immune Evasion. Trends Microbiol. 2018; 26(4):284–95. Epub 2018/02/18. https://doi.org/10.1016/j.tim.2018.01.007 PMID: 29452950
10. Camacho E, Vij R, Chrissian C, Prados-Rosales R, Gil D, O'Meally RN, et al. The structural unit of melanin in the cell wall of the fungal pathogen *Cryptococcus neoformans*. Journal of Biological Chemistry. 2019; 294(27):10471–89. https://doi.org/10.1074/jbc.RA119.008684 PMID: 31118223
11. O'Meara TR, Alspaugh JA. The *Cryptococcus neoformans* Capsule: a Sword and a Shield. 2012; 25 (3):387–408. https://doi.org/10.1128/CMR.00001-12 PMID: 22763631

12. Erwig LP, Gow NAR. Interactions of fungal pathogens with phagocytes. Nature Reviews Microbiology. 2016; 14(3):163–76. https://doi.org/10.1038/nrmicro.2015.21 PMID: 26853116

13. Ost KS, Esher SK, Leopold Wager CM, Walker L, Wagener J, Munro C, et al. Rim Pathway-Mediated Alterations in the Fungal Cell Wall Influence Immune Recognition and Inflammation. mBio. 2017; 8(1). Epub 2017/02/02. https://doi.org/10.1128/mBio.02290-16 PMID: 28143983;

14. Mahl CRA, Taketa TB, Rocha-Neto JBM, Almeida WP, Beppu MM. Copper Ion Uptake by Chitosan in the Presence of Amyloid-beta and Histidine. Appl Biochem Biotechnol. 2020; 190(3):949–65. Epub 2019/10/21. https://doi.org/10.1007/s12010-019-03120-z PMID: 31630339

15. Mullen DCW M.D., Beveridge T.J., Bailey G.W.,. Sorption of heavy metals by the soil fungi Aspergillus niger and Mucor rouxii,. Soil Biology and Biochemistry. 1992; 24(2):129–35. https://doi.org/10.1016/0038-0717(92)90268-3

16. Staudt MW, Kruzel EK, Shimizu K, Hull CM. Characterizing the role of the microtubule binding protein Bim1 in *Cryptococcus neoformans*. Fungal genetics and biology: FG & B. 2010; 47(4):310–7. Epub 2010/01/02. https://doi.org/10.1016/j.fgb.2009.12.010 PMID: 20044015

17. Harrington BJ, Hageage GJ Jr. Calcofluor White: A Review of its Uses and Applications in Clinical Mycology and Parasitology. Laboratory Medicine. 2003; 34(5):361–7. https://doi.org/10.1309/EPH2TDT8335GH0R3 %J Laboratory Medicine.

18. Dichtl K, Samantaray S, Wagener J. Cell wall integrity signalling in human pathogenic fungi. Cell Microbiol. 2016; 18(9):1228–38. Epub 2016/05/08. https://doi.org/10.1111/cmi.12612 PMID: 27155139

19. de Oliveira HC, Rossi SA, García-Barbazán I, Zaragoza Ó, Trevijano-Contador N. Cell Wall Integrity Pathway Involved in Morphogenesis, Virulence and Antifungal Susceptibility in *Cryptococcus neoformans*. Journal of fungi (Basel, Switzerland). 2021; 7(10). Epub 2021/10/24. https://doi.org/10.3390/jof7100831 PMID: 34682253

20. Kuranda K, Leberre V, Sokol S, Palamarczyk G, Francois J. Investigating the caffeine effects in the yeast *Saccharomyces cerevisiae* brings new insights into the connection between TOR, PKC and Ras/cAMP signalling pathways. Mol Microbiol. 2006; 61(5):1147–66. Epub 2006/08/24. https://doi.org/10.1111/j.1365-2958.2006.05300.x PMID: 16925551

21. Heilmann CJ, Sorgo AG, Mohammadi S, Sosinska GJ, de Koster CG, Brul S, et al. Surface stress induces a conserved cell wall stress response in the pathogenic fungus *Candida albicans*. Eukaryot Cell. 2013; 12(2):254–64. Epub 2012/12/18. https://doi.org/10.1128/EC.00278-12 PMID: 23243062

22. Baker LG, Specht CA, Donlin MJ, Lodge JK. Chitosan, the deacetylated form of chitin, is necessary for cell wall integrity in *Cryptococcus neoformans*. Eukaryot Cell. 2007; 6(5):855–67. Epub 2007/04/03. https://doi.org/10.1128/EC.00399-06 PMID: 17400891

23. Sun T-S, Ju X, Gao H-L, Wang T, Thiele DJ, Li J-Y, et al. Reciprocal functions of *Cryptococcus neoformans* copper homeostasis machinery during pulmonary infection and meningoencephalitis. Nature Communications. 2014; 5(1):5550. https://doi.org/10.1038/ncomms6550 PMID: 25417972

24. Walton FJ, Idnurm A, Heitman J. Novel gene functions required for melanization of the human pathogen *Cryptococcus neoformans*. Mol Microbiol. 2005; 57(5):1381–96. Epub 2005/08/17. https://doi.org/10.1111/j.1365-2958.2005.04779.x PMID: 16102007

25. Saikia S, Oliveira D, Hu G, Kronstad J, Deepe GS. Role of Ferric Reductases in Iron Acquisition and Virulence in the Fungal Pathogen *Cryptococcus neoformans*. 2014; 82(2):839–50. https://doi.org/10.1128/IAI.01357-13 PMID: 24478097

26. Jung WH, Kronstad JW. Iron and fungal pathogenesis: a case study with *Cryptococcus neoformans*. Cell Microbiol. 2008; 10(2):277–84. Epub 2007/11/29. https://doi.org/10.1111/j.1462-5822.2007.01077.x PMID: 18042257

27. Kronstad JW, Hu G, Jung WH. An encapsulation of iron homeostasis and virulence in *Cryptococcus neoformans*. Trends Microbiol. 2013; 21(9):457–65. Epub 2013/07/03. https://doi.org/10.1016/j.tim.2013.05.007 PMID: 23810126

28. Mukaremera L, Lee KK, Wagener J, Wiesner DL, Gow NAR, Nielsen K. Titan cell production in *Cryptococcus neoformans* reshapes the cell wall and capsule composition during infection. The Cell Surface. 2018; 1:15–24. https://doi.org/10.1016/j.tcsw.2017.12.001 PMID: 30123851

29. Dambuza IM, Drake T, Chapuis A, Zhou X, Correia J, Taylor-Smith L, et al. The *Cryptococcus neoformans* Titan cell is an inducible and regulated morphotype underlying pathogenesis. PLoS Pathog. 2018; 14(5):e1006978. Epub 2018/05/19. https://doi.org/10.1371/journal.ppat.1006978 PMID: 29775474

30. Chrissian C, Camacho E, Fu MS, Prados-Rosales R, Chatterjee S, Cordero RJB, et al. Melanin deposition in two *Cryptococcus* species depends on cell-wall composition and flexibility. J Biol Chem. 2020; 295(7):1815–28. Epub 2020/01/04. https://doi.org/10.1074/jbc.RA119.011949 PMID: 31896575

31. Kim JM, Baars O, Morel FM. Bioavailability and Electroreactivity of Zinc Complexed to Strong and Weak Organic Ligands. Environmental science & technology. 2015; 49(18):10894–902. Epub 2015/08/08. https://doi.org/10.1021/acs.est.5b02098 PMID: 26252068

32. Figueroa-López AM, Cordero-Ramírez JD, Quiroz-Figueroa FR, Maldonado-Mendoza IE. A high-throughput screening assay to identify bacterial antagonists against *Fusarium verticillioides*. Journal of basic microbiology. 2014; 54 Suppl 1:S125–33. Epub 2013/06/22. https://doi.org/10.1002/jobm.201200594 PMID: 23787812

33. Ryva B, Zhang K, Asthana A, Wong D, Vicioso Y, Parameswaran R. Wheat Germ Agglutinin as a Potential Therapeutic Agent for Leukemia. Frontiers in oncology. 2019; 9:100. Epub 2019/03/09. https://doi.org/10.3389/fonc.2019.00100 PMID: 30847305

34. Ost KS, O'Meara TR, Huda N, Esher SK, Alspaugh JA. The *Cryptococcus neoformans* alkaline response pathway: identification of a novel rim pathway activator. PLoS Genet. 2015; 11(4):e1005159. Epub 2015/04/11. https://doi.org/10.1371/journal.pgen.1005159 PMID: 25859664

35. Esher SK, Ost KS, Kohlbrenner MA, Pianalto KM, Telzrow CL, Campuzano A, et al. Defects in intracellular trafficking of fungal cell wall synthases lead to aberrant host immune recognition. PLOS Pathogens. 2018; 14(6):e1007126. https://doi.org/10.1371/journal.ppat.1007126 PMID: 29864141

36. Ding C, Yin J, Tovar EM, Fitzpatrick DA, Higgins DG, Thiele DJ. The copper regulon of the human fungal pathogen *Cryptococcus neoformans* H99. Mol Microbiol. 2011; 81(6):1560–76. Epub 2011/08/09. https://doi.org/10.1111/j.1365-2958.2011.07794.x PMID: 21819456

37. Pianalto KM, Billmyre RB, Telzrow CL, Alspaugh JA. Roles for Stress Response and Cell Wall Biosynthesis Pathways in Caspofungin Tolerance in *Cryptococcus neoformans*. Genetics. 2019; 213(1):213–27. Epub 2019/07/04. https://doi.org/10.1534/genetics.119.302290 PMID: 31266771;

38. Walker LA, Munro CA, de Bruijn I, Lenardon MD, McKinnon A, Gow NAR. Stimulation of Chitin Synthesis Rescues *Candida albicans* from Echinocandins. PLOS Pathogens. 2008; 4(4):e1000040. https://doi.org/10.1371/journal.ppat.1000040 PMID: 18389063

39. Fortwendel JR, Juvvadi PR, Perfect BZ, Rogg LE, Perfect JR, Steinbach WJ. Transcriptional regulation of chitin synthases by calcineurin controls paradoxical growth of *Aspergillus fumigatus* in response to caspofungin. Antimicrobial agents and chemotherapy. 2010; 54(4):1555–63. Epub 2010/02/04. https://doi.org/10.1128/AAC.00854-09 PMID: 20124000

40. Frases S, Pontes B, Nimrichter L, Viana NB, Rodrigues ML, Casadevall A. Capsule of *Cryptococcus neoformans* grows by enlargement of polysaccharide molecules. 2009; 106(4):1228–33. https://doi.org/10.1073/pnas.0808995106 %J Proceedings of the National Academy of Sciences. PMID: 19164571

41. Jiang N, Sun N, Xiao D, Pan J, Wang Y, Zhu X. A copper-responsive factor gene CUF1 is required for copper induction of laccase in *Cryptococcus neoformans*. FEMS microbiology letters. 2009; 296(1):84–90. Epub 2009/05/23. https://doi.org/10.1111/j.1574-6968.2009.01619.x PMID: 19459959

42. Ding C, Festa RA, Chen YL, Espart A, Palacios Ò, Espín J, et al. *Cryptococcus neoformans* copper detoxification machinery is critical for fungal virulence. Cell host & microbe. 2013; 13(3):265–76. Epub 2013/03/19. https://doi.org/10.1016/j.chom.2013.02.002 PMID: 23498952

43. Li C, Li Y, Ding C. The Role of Copper Homeostasis at the Host-Pathogen Axis: From Bacteria to Fungi. Int J Mol Sci. 2019; 20(1):175. https://doi.org/10.3390/ijms20010175 PMID: 30621285

44. Garcia-Santamarina S, Uzarska MA, Festa RA, Lill R, Thiele DJ. *Cryptococcus neoformans* Iron-Sulfur Protein Biogenesis Machinery Is a Novel Layer of Protection against Cu Stress. mBio. 2017 2017/10//; 8(5). https://doi.org/10.1128/mBio.01742-17 PMID: 29089435

45. Sun T, Li Y, Li Y, Li H, Gong Y, Wu J, et al. Proteomic Analysis of Copper Toxicity in Human Fungal Pathogen *Cryptococcus neoformans*. 2021; 11(747). https://doi.org/10.3389/fcimb.2021.662404

46. Sun T, Li X, Song W, Yu S, Wang L, Ding C, et al. Metabolomic alterations associated with copper stress in *Cryptococcus neoformans*. Future Microbiol. 2021; 16:305–16. Epub 2021/02/27. https://doi.org/10.2217/fmb-2020-0290 PMID: 33635120

47. Broxton CN, Culotta VC. An Adaptation to Low Copper in *Candida albicans* Involving SOD Enzymes and the Alternative Oxidase. PLOS ONE. 2016; 11(12):e0168400. https://doi.org/10.1371/journal.pone.0168400 PMID: 28033429

48. Kropat J, Gallaher SD, Urzica EI, Nakamoto SS, Strenkert D, Tottey S, et al. Copper economy in *Chlamydomonas*: prioritized allocation and reallocation of copper to respiration vs. photosynthesis. Proc Natl Acad Sci U S A. 2015; 112(9):2644–51. Epub 2015/02/04. https://doi.org/10.1073/pnas.1422492112 PMID: 25646490

49. Smith AD, Garcia-Santamarina S, Ralle M, Loiselle DR, Haystead TA, Thiele DJ. Transcription factor-driven alternative localization of *Cryptococcus neoformans* superoxide dismutase. J Biol Chem. 2021; 296:100391. Epub 2021/02/11. https://doi.org/10.1016/j.jbc.2021.100391 PMID: 33567338

50. Chen X, Tian Z, Cheng H, Xu G, Zhou H. Adsorption process and mechanism of heavy metal ions by different components of cells, using yeast (*Pichia pastoris*) and Cu(2+) as biosorption models. RSC advances. 2021; 11(28):17080–91. Epub 2022/04/29. https://doi.org/10.1039/d0ra09744f PMID: 35479686

51. Ipsen JØ, Hallas-Møller M, Brander S, Lo Leggio L, Johansen KS. Lytic polysaccharide monooxygenases and other histidine-brace copper proteins: structure, oxygen activation and biotechnological applications. Biochemical Society Transactions. 2021; 49(1):531–40. https://doi.org/10.1042/BST20201031%J Biochemical Society Transactions. PMID: 33449071

52. Rani Singhania R, Dixit P, Kumar Patel A, Shekher Giri B, Kuo C-H, Chen C-W, et al. Role and significance of lytic polysaccharide monooxygenases (LPMOs) in lignocellulose deconstruction. Bioresource Technology. 2021; 335:125261. https://doi.org/10.1016/j.biortech.2021.125261 PMID: 34000697

53. Black B, Lee C, Horianopoulos LC, Jung WH, Kronstad JW. Respiring to infect: Emerging links between mitochondria, the electron transport chain, and fungal pathogenesis. PLoS pathogens. 2021; 17(7): e1009661–e. https://doi.org/10.1371/journal.ppat.1009661 PMID: 34237096

54. Da Silva CA, Hartl D, Liu W, Lee CG, Elias JA. TLR-2 and IL-17A in chitin-induced macrophage activation and acute inflammation. Journal of immunology (Baltimore, Md: 1950). 2008; 181(6):4279–86. Epub 2008/09/05. https://doi.org/10.4049/jimmunol.181.6.4279 PMID: 18768886

55. Da Silva CA, Chalouni C, Williams A, Hartl D, Lee CG, Elias JA. Chitin is a size-dependent regulator of macrophage TNF and IL-10 production. Journal of immunology (Baltimore, Md: 1950). 2009; 182 (6):3573–82. Epub 2009/03/07. https://doi.org/10.4049/jimmunol.0802113 PMID: 19265136

56. Hole CR, Lam WC, Upadhya R, Lodge JK. *Cryptococcus neoformans* Chitin Synthase 3 Plays a Critical Role in Dampening Host Inflammatory Responses. mBio. 2020; 11(1). Epub 2020/02/20. https://doi.org/10.1128/mBio.03373-19 PMID: 32071275

57. Hembach L, Bonin M, Gorzelanny C, Moerschbacher BM. Unique subsite specificity and potential natural function of a chitosan deacetylase from the human pathogen *Cryptococcus neoformans*. Proc Natl Acad Sci U S A. 2020; 117(7):3551–9. Epub 2020/02/06. https://doi.org/10.1073/pnas.1915798117 PMID: 32015121

58. Toffaletti DL, Rude TH, Johnston SA, Durack DT, Perfect JR. Gene transfer in *Cryptococcus neoformans* by use of biolistic delivery of DNA. Journal of bacteriology. 1993; 175(5):1405–11. Epub 1993/03/01. https://doi.org/10.1128/jb.175.5.1405-1411.1993 PMID: 8444802